The Meteorological Magazine

March 1992

Assessment of model fluxes
Traffic accidents in hail showers

DUPLICATE JOURNALS

National Meteorological Library
FitzRoy Road, Exeter, Devon. EX1 3PB

HMSO

Met.O.1004 Vol. 121 No. 1436

© Crown copyright 1992.
Applications for reproduction should be made to HMSO.

First published 1992

HMSO publications are available from:

HMSO Publications Centre
(Mail and telephone only)
PO Box 276, London, SW8 5DT
Telephone orders 071-873 9090
General enquiries 071-873 0011
(queuing system in operation for both numbers)

HMSO Bookshops
49 High Holborn, London, WC1V 6HB 071-873 0011 (counter service only)
258 Broad Street, Birmingham, B1 2HE 021-643 3740
Southey House, 33 Wine Street, Bristol, BS1 2BQ (0272) 264306
9–21 Princess Street, Manchester, M60 8AS 061-834 7201
80 Chichester Street, Belfast, BT1 4JY (0232) 238451
71 Lothian Road, Edinburgh, EH3 9AZ 031-228 4181

HMSO's Accredited Agents
(see Yellow Pages)

and through good booksellers

3 8078 0010 2478 7

The
Meteorological Magazine

March 1992
Vol. 121 No. 1436

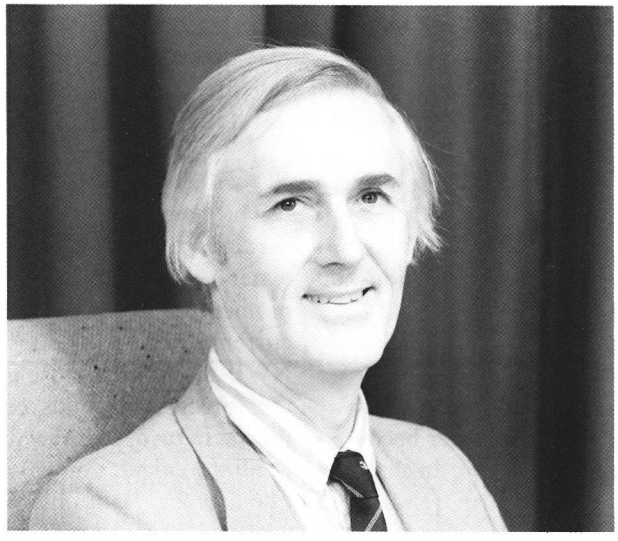

Appointment of Chief Executive of the Meteorological Office

Professor Julian Hunt, MA, PhD, FIMA, FRMetS, FRS was appointed to succeed Sir John Houghton as Chief Executive of the Meteorological Office from 1 January 1992.

Professor Hunt was previously Professor of Fluid Dynamics with the University of Cambridge's Department of Applied Mathematics and Theoretical Physics. Recently he has been involved in a project with his University, the Meteorological Office and National Power to develop an advanced method of calculating dispersion in the atmosphere and also making more use of the advances in meteorological understanding. He held a Readership there from 1978 to 1990, when he was promoted to a Personal Chair. He was elected a Fellow of the Royal Society in 1989.

Professor Hunt, now 50, was a pupil at Westminster School and then gained First Class Honours in Mechanical Sciences at the University of Cambridge. He was awarded his PhD for his work on Aspects of Magnetohydrodynamics.

His appointment reflects the importance the Meteorological Office attaches to retaining the high professional and scientific standards for which it is noted throughout the world.

Professor Hunt's impressive career has fitted him superbly to direct further improvements in forecast accuracy, and research into climate change. His management and commercial experience will also be invaluable: the Meteorological Office as an Executive Agency must satisfy a vast range of technical and financial requirements.

Professor Hunt, accepting the appointment, said:

For a large part of my career I have been intimately involved in scientific research allied to meteorology. I am delighted and honoured to have been chosen as Chief Executive of such a prestigious organization. I have for many years been impressed by the developing range of high-quality services provided by the Meteorological Office to its clients, as well as to the quality of its research. The Office has a well deserved international reputation of the highest order and I am excited at the prospect of becoming identified with it.

Ocean Forecasting

Nina Morgan
Science writer

1. Introduction

Ocean forecasting lags far behind atmospheric weather forecasting. In theory the oceans and the atmosphere obey the same physical laws, but in practice, ocean forecasting has some special requirements.

People who depend on the land for their livelihood can rely on daily, detailed, accurate forecasts of the weather thanks to the development of numerical weather prediction (NWP) methods which use mathematical models, real-time weather observations and large computers which project motions of the atmosphere forward in time-steps using physical equations.

The Royal Navy, concerned with events in the oceans, require detailed daily ocean forecasts, and those which give information about temperature and salinity throughout the ocean depths. Horizontal resolutions of 10 km or less for these ocean models will probably not be available before the end of the century.

2. Related circulation systems

The oceans, which cover more than 70% of the Earth's surface, have a great influence on the weather because they act as a huge heat and moisture reservoir. In climate modelling, which concentrates on long-term trends, the effects of clouds and the oceans are two major unknowns. Because ocean circulation occurs over a very long time-scale, ocean models are commonly coupled to climate models.

3. Important differences

The ocean and the atmosphere interact at the sea surface by exchanging fluxes of momentum, heat and moisture across the sea–air interface. There are, however, some important differences between atmospheric and ocean circulation systems which affect the way their behaviour can be modelled.

Atmospheric circulation is driven by heat from the Sun and the Earth's rotation with pressure systems ranging up to thousands of kilometres wide. Ocean circulation is driven primarily by fluxes of heat (including heat from the sun), fresh water, and momentum, or wind stress, at the interface between the air and the sea surface. The oceanic equivalent of atmospheric pressure systems are on scales of tens to hundreds of kilometres. Therefore, accurate modelling of ocean systems requires a higher resolution than that needed to model the atmosphere. This, in turn, requires greater computing power.

4. Improving ocean forecasts

Models suitable for ocean forecasting are being used for long-term ocean climate studies. Input of the surface fluxes; heat, moisture and momentum, calculated from atmospheric NWP forecasts, is essential. The quality of these flux data from the NWP must be very high, and this can be achieved by iterative changes to the flux equations.

Further improvements will come with more accurate real-time weather data gathered from global weather observations. Weather stations are particularly sparse over the oceans, but the new generation of meteorological satellites, such as the recently launched ERS-1, will help to fill the data gap.

5. Quality of fluxes

The three major fluxes which influence the ocean models are heat (which affects ocean temperature), fresh water (which affects the salinity of the ocean), and momentum (or wind stress) which drives the ocean currents. The forecasts and the fluxes produced by NWP models are closely interlinked. The accuracy of the forecasts depends on the calculation of accurate fluxes. In turn, more accurate forecasts will lead to more accurate calculation of fluxes. The formulae used to calculate the fluxes in NWP models are approximations, which give results that may have significant errors.

In 1991, J.O.S. Alves of the Meteorological Office suggested improvements to the calculation of momentum fluxes in the North Atlantic (*Meteorological Magazine*, November 1991). In this issue, he goes on to analyse the problems involved in accurate calculation of heat and fresh-water fluxes.

Many of Alves' suggestions have already been incorporated in the new Meteorological Office Unified Model. His next task will be to assess the fluxes in the Unified Model. Suggestions made by Alves for improvements in the formulae for calculating fluxes will be relevant to all oceans, even though the study concentrated on analyses of North Atlantic fluxes.

6. Help for oceanographers

The work done by Alves is part of the FOAM (Forecasting Ocean Atmosphere Model) project at the Meteorological Office. The project aims to introduce daily ocean forecasts from an ocean model by the mid 1990s. Further improvements in resolution, for example, to that of the mesoscale weather forecast model grid used by the Meteorological Office, will require more-accurate measurements of the state of the ocean each day and greater computing power than currently available.

To prepare accurate forecasts for the Royal Navy, who are primarily interested in the surface layers, the

multilayered model will be run throughout the ocean depth extending to about 6 km below the ocean surface. As a spin-off, this complete 3-dimensional coverage of the oceans will provide valuable information to oceanographers interested in studying ocean circulation.

7. Looking forward to the past

An improved fine-resolution ocean model will lead to a greater understanding of the factors which influence ocean circulation, making it possible to unravel ocean circulation patterns associated with climate change in the geological past. For example, it has been suggested that circulation patterns in the Atlantic were very different during the last ice age from what they are today.

A better understanding of the interaction between ocean circulation and climate in both the present and the past will help to predict the climate in the future.

551.509.313:551.509.5:551.551.8(26)

An assessment of the surface fluxes from the Meteorological Office numerical weather prediction models. Part II: Heat and fresh water

J.O.S. Alves
Meteorological Office, Bracknell

Summary

Interaction between the ocean and the atmosphere is brought about by the exchange of fluxes of momentum, heat and moisture across their interface. Estimates of these come from numerical weather prediction models. Surface heat and moisture fluxes from the Meteorological Office's fine- and coarse-mesh models are assessed and their parametrizations reviewed. The response of the ocean to these fluxes and any biases they may have is investigated using an ocean model of the North Atlantic.

1. Introduction

Fluxes of heat, momentum and fresh water are exchanged between the ocean and atmosphere. An ocean forecasting model is being developed by the FOAM group (Forecasting Ocean Atmosphere Model) of the Meteorological Office (MO). This model will require the specification of the surface fluxes, up to six days ahead of time, as its upper boundary condition. The only source of forecast surface fluxes, i.e. estimates of the surface fluxes ahead of time, is NWP (Numerical Weather Prediction) models. As a first stage in the development of FOAM an assessment of the surface fluxes from the current MO operational NWP models has been carried out. The results for the heat and fresh water fluxes form the contents of this document. A similar paper by Alves (1991) reports on the assessment of the surface momentum fluxes.

Three main types of error can occur in the surface fluxes from a NWP model. The forecast error depends on the ability of the model to represent the real atmospheric situation and to forecast it correctly. Such errors will be ignored as the main interest is in the calculation of the surface fluxes themselves. A second source of errors is the parametrization of the fluxes from the model fields. Thirdly, the model parametrizes the surface fluxes as functions of the basic model fields; wind, temperature and humidity. Calculation of the radiation fluxes is also sensitive to the parametrization of other physical processes, such as the representation of cloud and convection, which themselves depend on the basic model fields. The representation of the basic fields in the NWP models will be discussed briefly.

An ocean model was used to assess the quality of the surface fluxes. The aim was to reveal any biases in the surface fluxes and to quantify the sensitivity of the ocean model to these biases by comparing results from ocean model integrations using the NWP fluxes with similar integrations using climatological fluxes. Fluxes from the two MO operational models were compared and their parametrizations were discussed.

A brief description of the operational NWP models used by the MO and a fuller description of how they parametrize the surface fluxes is given in section 2. Section 3 describes the ocean model and the experiments carried out. Results from the ocean model test,

including a discussion of the flux parametrizations, for the heat fluxes (excluding solar), solar heat flux and fresh water flux are given in sections 4, 5 and 6 respectively. In section 7 a summary is presented and conclusions are drawn.

2. The NWP models

2.1 The MO NWP models

The MO used two fully operational numerical weather prediction models, described by Bell and Dickinson (1987). The 'Coarse-Mesh' (CM) model is global and used a latitude/longitude resolution of 1.875° × 1.5°. The 'Fine-Mesh' (FM) model had twice the resolution of the CM, this being 0.9375° × 0.75°, and covered an area from 30° N to 80° N and from 40° E to 80° W. Output from the global CM model was used to supply boundary conditions for the limited-area FM model. Both models were run twice a day, at 0000 UTC and 1200 UTC. The CM model produced forecasts up to six days ahead and the FM model up to 36 hours ahead. Only the first twelve hours of each forecast were used in this study.

From each model, monthly mean fields consisting of the first twelve hours of each forecast were formed for the month of October 1989. The fields available from the NWP archives are shown in the Table I.

Table I. Fields extracted from NWP archives. X = not available

	FM	CM
σ_1, temperature	✓	X
Surface temperature	✓	✓
σ_1, relative humidity	✓	✓
Precipitation minus evaporation	✓	✓
Latent heat flux	✓	✓
Sensible heat flux	✓	✓
Net surface solar radiation	✓	✓
Net surface IR radiation	✓	✓
σ_1, wind components	✓	X
10-metre wind components	✓	✓

2.2 Parametrization of the surface processes.

The parametrization of the boundary-layer processes is described fully in Bell and Dickinson (1987). A brief summary and modifications are outlined below. The surface latent heat flux (λE), evaporation rate (E) and sensible heat flux (H) were defined in terms of bulk aerodynamic formulae. For the CM model the bulk formulae took the explicit form

$$H = -\rho c_p C_H |v_1| (\theta_1 - \theta_*) \quad (1)$$

$$\lambda E = -\rho \lambda C_E |v_1| (q_1 - q_s(\theta_*)) \quad (2)$$

where C_H is the exchange coefficient for heat, C_E is the exchange coefficient for moisture, $|v| = (u_1^2 + v_1^2)^{1/2}$, u_1 and v_1 are the first model-level horizontal wind components, θ_1 is the first sigma-level model potential temperature, θ_* is the sea-surface potential temperature (the sea surface temperature was kept constant throughout each NWP model integration), λ is the latent heat of vaporization, q_1 is the specific humidity at the model's first sigma level and $q_s(\theta_*)$ is the saturated specific humidity at the potential temperature θ_* (given by Clausius–Clapeyron relation). In the FM model an implicit finite difference scheme (Kitchen 1986) was used for the turbulent fluxes in the boundary layer and the bulk aerodynamic formulae took the form

$$H = -\rho c_p C_H |v_1| \{\alpha(\theta_1^{t+\Delta t} - \theta_*) + (1-\alpha)(\theta_1^{t} - \theta_*)\}$$

$$\lambda E = -\rho \lambda C_E |v_1| (\alpha(q_1^{t+\Delta t} - q_s(\theta_*)) + (1-\alpha)(q_1^{t} - q_s(\theta_*))$$

where $\alpha = 0.5$ and the superscripts t and $t+\Delta t$ refer to successive time levels; Δt represents a time-step.

The exchange coefficients C_H and C_E depend on the surface roughness length z_o and the bulk Richardson number Ri_B. They were calculated using empirical functions which depend on the stability of the boundary layer (see Bell and Dickinson (1987)). Bell and Dickinson indicate that in the CM model z_o over the sea was a constant value of 10^{-4} m. For the FM model the surface roughness length z_o was a variable and was calculated using the Charnock formula (Charnock 1955)

$$z_o = M u_*^2 / g$$

where M is a constant (taken to be 0.019), u_* is the surface friction speed and g is the acceleration due to gravity.

2.3 The parametrization of the radiative fluxes

Net infrared radiation flux at the sea surface was calculated by the difference between the upward long-wave radiation flux from the sea surface (assumed to be a black body) and downward long-wave flux (see Bell and Dickinson (1987) for full details). The downward long-wave flux at the surface was a combination of the clear sky downward flux and the downward flux from the cloud base. In the CM model the cloud distribution was taken to be a zonally averaged climatology. In the FM model an interactive cloud scheme was used where for each model layer the fraction of cloud cover Q is calculated from the relative humidity field (for relative humidity $H > H_{crit}$) from the equation

$$Q = (H - H_{crit})^2 / (1 - H_{crit})$$

where H_{crit} is taken to be 0.85. Clouds are then divided into 'low', 'medium' and 'high' by finding the largest

value of Q in each of three bands of model layers. Convective cloud was diagnosed from the convection scheme and was treated as a fourth cloud type by the radiation scheme. Clear sky downward flux was calculated taking into account the absorption by water vapour, carbon dioxide and ozone (see Bell and Dickinson (1987) for full details). Water vapour distribution was obtained from the models humidity field and the carbon dioxide was assumed to be well mixed throughout the atmosphere (mixing ratio of 4.9×10^{-4} kg kg^{-1}). Ozone mixing ratios were specified above 200 mb from monthly climatological zonally averaged values (Bolton 1981).

In the CM model the solar radiation flux reaching the surface was calculated by taking into account absorption by cloud whose distribution was given by a zonally averaged climatology. The FM model had a solar radiation scheme which took account of the diagnosed cloud (Bell and Dickinson 1987). The total downward short-wave radiation flux at some height z is given by

$$S(z) = (1-Q)S^{\infty}(z) + Q\Lambda S^{CL}(z)$$

where Q is the fractional cloud cover, $S^{\infty}(z)$ is the clear-sky radiation flux at height z, $S^{CL}(z)$ is the diffuse flux from the cloud and Λ is the transmissivity of the cloud. The clear-sky radiation flux $S^{\infty}(z)$ was calculated by taking into account absorption by three gases: water vapour, carbon dioxide and ozone. Where there was cloud $S^{CL}(z)$ was used which additionally incorporated the effect of diffusion by the cloud. A further adjustment took account of scattering by the atmosphere which is particularly important for low solar elevation.

A fraction α (the surface albedo) of the solar radiation reaching the sea surface was reflected back into the atmosphere. Over the sea and in clear sky conditions $\alpha = \alpha_o$ where $\alpha_o = 0.06$. When there was cloud present there would be multiple reflection of the solar radiation between the bottom of the cloud and the sea surface. This multiple reflection was taken into account by putting $\alpha = \alpha_{eff}$ (effective albedo) where α_{eff} is given by

$$\alpha_{eff} = \alpha_o(1-Q\beta)/(1-Q\beta\alpha_o)$$

where Q is an ensemble cloud amount and β an ensemble reflectivity incorporating the four types of cloud; low, medium, high and convective (see Bell and Dickinson (1987)).

2.4 Parametrization of precipitation

Precipitation was calculated in two forms; dynamic and convective. Dynamic rain was calculated using the model's humidity field. For each model layer where the specific humidity was greater than the saturated specific humidity for that particular layer, excess water was removed as precipitation taking into account changes in temperature due to latent heat release. Precipitation falling from one layer through another which was not saturated was evaporated (approximately 7 mm day^{-1}/100 mb). Precipitation at the surface was therefore the sum of precipitation less evaporation for all the model layers (note precipitation and evaporation do not occur on the same layer). Bell and Dickinson (1987) give a more detailed account of the calculation of the dynamic precipitation rates.

Convective precipitation rate was calculated using parameters from the model's convection scheme which was based on parcel theory modified by entrainment and detrainment (see Bell and Dickinson (1987) for more details). Condensation of cloud water occurred if the depth of the convective cloud was greater than a critical value D_{crit} (4 km over land, 1.5 km over sea and 1 km if the temperature of the layer above was less than 263 K) and the specific humidity is greater than a critical value q_{crit} (the smaller of 1 g kg^{-1} or saturated specific humidity). The precipitation rate was proportional to the difference between the specific humidity and the critical value q_{crit}, and the vertical mass flux in the convective plume. Rain falling from the cloud base was evaporated at a rate proportional to the difference between the specific humidity and the saturated specific humidity in the layers between the cloud base and the surface. The remaining precipitation determined the surface convective precipitation rate.

3. Use of an ocean model to assess the surface fluxes

The ocean model used is based on that of Cox (1984) and is described by Alves (1991). It uses regular latitude/longitude horizontal co-ordinates with a grid spacing of 1° throughout. In the mixed layer a scheme similar to that of Kraus and Turner (1967) is used. In this scheme convective mixing takes place when there is surface cooling. After this, or where there is net surface heating, the mixing energy of the wind is used to overcome the stability of the upper layers and mix the more buoyant water downwards. A mixed layer depth is diagnosed as the depth to which mixing occurs.

Surface fluxes of momentum, non-penetrating heat, solar radiation and fresh water are used as the upper boundary conditions for ocean model integrations. Momentum flux is used by the ocean model to drive the Ekman drift currents and the long-term average wind stress drives the upper-ocean circulation. Water near the surface is mixed downwards using the wind mixing energy. Heat is either input or removed from the ocean through the specification of the heat flux. The salt budget is modified at the surface by the fresh water flux.

For the month of October 1989 forcing fields were extracted from the NWP archives for each forecast starting at 00 UTC and 12 UTC each day. The T+3, T+6, T+9 and T+12 forecasts from the FM model were used to form three-hourly averaged forcing fields. For the CM model only the T+6 and the T+12 fields were available. The T+6 was copied and relabelled the T+3 and the T+12 was copied and relabelled the T+9, so

forming a set of three-hourly forcing fields. The fields extracted consisted of the surface sensible heat flux, latent heat flux, infrared radiation, solar radiation and precipitation minus evaporation (PME). Sensible heat, latent heat and infrared radiative fluxes were combined to form the non-penetrative surface heat flux (note that this excludes the solar radiation as this penetrates into the upper few tens of metres of the ocean).

The ocean model's domain covers the Atlantic from 30°S to 80°N. The region covered by the FM is contained within the domain of the ocean model. It is desirable to use the FM model's forcing fields where possible because of its improved physics and higher resolution. To achieve this the FM and CM fields were merged together so that the FM values were used within the FM domain and those of the CM outside the FM domain, with a smoothing applied at the FM boundary. The resulting fields will be from hereon referred to as the 'merged' fields.

The ocean model was integrated using climatological fluxes for seven months as described by Alves (1991). Similar integrations to those carried out by Alves for the NWP momentum fluxes were repeated for each of the fluxes: non-penetrative heat flux (excluding solar), solar radiation flux and the PME flux, where the climatological flux was exchanged with one of the NWP fluxes, for October 1989, in each experiment. In the following sections these will be referred to as the 'NWP' runs or the 'operational' runs. Monthly mean fields for temperature, salinity, currents, mixed layer depth and the forcing fields were obtained for each run and compared with the climatological control run. These will be discussed in the sections to follow. For the purpose of comparison all fields presented which are not from the ocean model have been interpolated onto the ocean model's grid.

4. Non-penetrative heat fluxes

4.1 Results

The monthly mean latent heat flux for October 1989 from the CM model is shown in Fig. 1(a). Areas of maximum latent heat flux are in general associated with northward transport of warm water within the Atlantic Ocean. Maximum latent heat flux occurs in the Gulf Stream region and reaches 300 W m^{-2}. When compared with a climatology (Esbensen and Kushnir 1981), Fig. 1(b), the CM model latent heat flux shows differences of up to 50 W m^{-2} in areas not influenced by strong oceanic heat transport. In the Gulf Stream region itself the CM model exceeds the climatology by up to 100 W m^{-2} (33%), but away from the main thermal gradients associated with the Gulf Stream the CM has a smaller heat flux than the climatology. This appears to be a consequence of the better resolution of the Gulf Stream thermal gradients in the SST field used by the operational models compared with that used to calculate the Esbensen and Kushnir fluxes (on a 5° × 5° grid). Comparing the FM and CM models' latent heat flux (Fig. 2), the FM exceeds the CM by up to 40 W m^{-2} (13%) in the Gulf Stream region. Away from the western Atlantic the differences between the two models is smaller and generally less than 20 W m^{-2}.

Fig. 3(a) shows the monthly mean sensible heat flux for October 1989 produced by the CM model. Throughout the tropical Atlantic the sensible heat flux is small, generally less than 20 W m^{-2} and from the ocean to the atmosphere. In the middle latitudes (North Atlantic) the heat flux shows a larger variability and reaches up to 60 W m^{-2} in the region influenced by the Gulf Stream. Large heat fluxes near the Gulf Stream arise due to cold air flowing across the Gulf Stream from the cold shelf waters into the warm open ocean. Similarly in the extreme north of the domain, large heat fluxes with great variability occur as cold air from the snow and ice covered sea and land flows over the relatively warmer open sea. When compared with the climatology (see Fig. 3(b)) the sensible heat flux from the CM model agrees to within 10 W m^{-2} or so in the tropical ocean, although this is of the same magnitude as the heat flux itself. In the middle latitudes the variability in the difference is large. In the Gulf Stream region the sensible heat flux is up to 45 W m^{-2} (65%) larger than the climatology but is partly due to a better resolution of the SST used by the operational models. The FM model when compared with the CM model (not shown) indicates differences of up to 10 W m^{-2}; the maximum heat flux in the CM model occurs in the mid-latitude western Atlantic and this is simulated by the FM model to be 15% larger.

Monthly mean infrared radiation (IR) from the CM model for October 1989 is shown in Fig. 4(a). The net upward IR flux ranges from 30 to 80 W m^{-2} throughout the whole domain with the maximum occurring in the western Atlantic in the region influenced by the Gulf Stream. Since the IR radiation scheme uses a zonally averaged climatological cloud distribution, the main zonal variability in the IR flux comes from the variability in the SST (sea surface assumed to be black body). Fig. 4(b) shows the IR radiation from the CM model less a climatological field (Esbensen and Kushnir 1981). The CM model has a larger upward IR flux on the western tropical South Atlantic but less on the eastern tropical South Atlantic. Over the whole of the tropical North Atlantic the CM model has a larger IR radiation flux, up to 30 W m^{-2} (50%) more than the climatology. In the middle latitudes, north of about 45°N the CM model has a smaller IR radiation flux than climatology and vice versa south of 45°N. However, in the western Atlantic the Gulf Stream appears to be a divide, with the western side having a smaller IR than the climatology and the warmer waters of the eastern side having a larger IR flux than the climatology. This again emphasizes the better-resolved SST field used by the operational models. The FM model when compared with the CM (Fig. 5) shows a field with a greater zonal variability as a result of the use of an interactive cloud scheme. In the

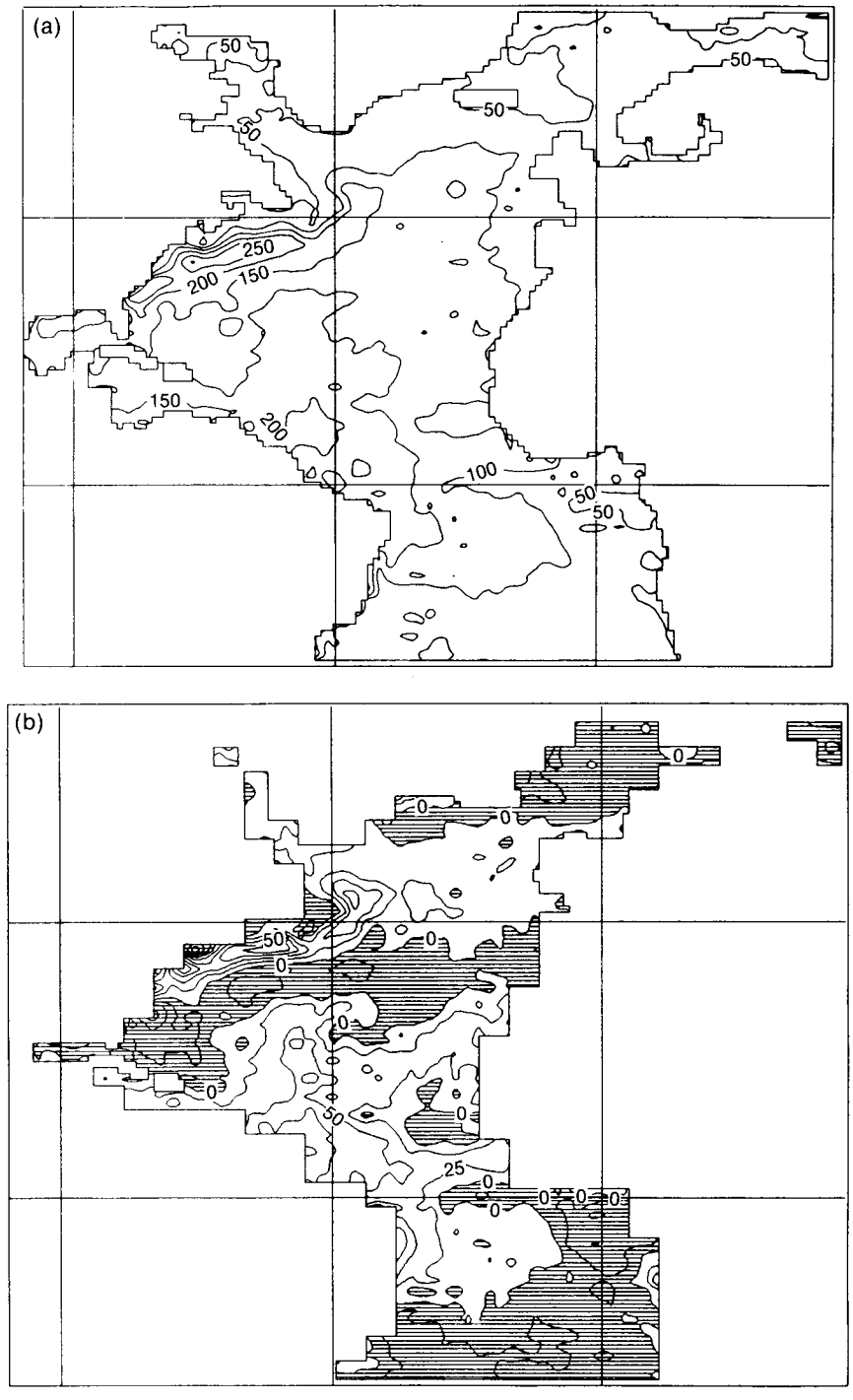

Figure 1. (a) Coarse-mesh monthly mean latent heat flux for October 1989 with contours every 50 W m^{-2}. (b) Difference between the monthly mean latent heat flux from the course-mesh model and climatology. Contours every 25 W m^{-2} with negative areas shaded.

northern and southernmost parts of the FM domain the FM model has a smaller IR flux than the CM (for example 10 W m^{-2}, 25% smaller west of Iceland). Elsewhere the FM has a larger IR flux, for example, 25 W m^{-2} (50%) larger in parts of the mid-latitude west Atlantic.

The three heat fluxes above were combined to form a net non-penetrative heat flux from the operational FM and CM models. An ocean model was integrated with the operational non-penetrative heat flux and all other fluxes being a climatology. Although the influence of each of the separate fluxes above was not tested separately with an ocean model integration, the sensitivity to the net heat flux can be thought of as representing the sensitivity to each of the individual heat fluxes.

Fig. 6(a) shows the climatological heat flux used for the climatological control run. The field is very smooth with the upward heat flux increasing as one moves westwards and towards the tropical North Atlantic. The maximum heat flux occurs in the Gulf Stream region where it reaches 300 W m^{-2}. Fig. 6(b) shows the merged

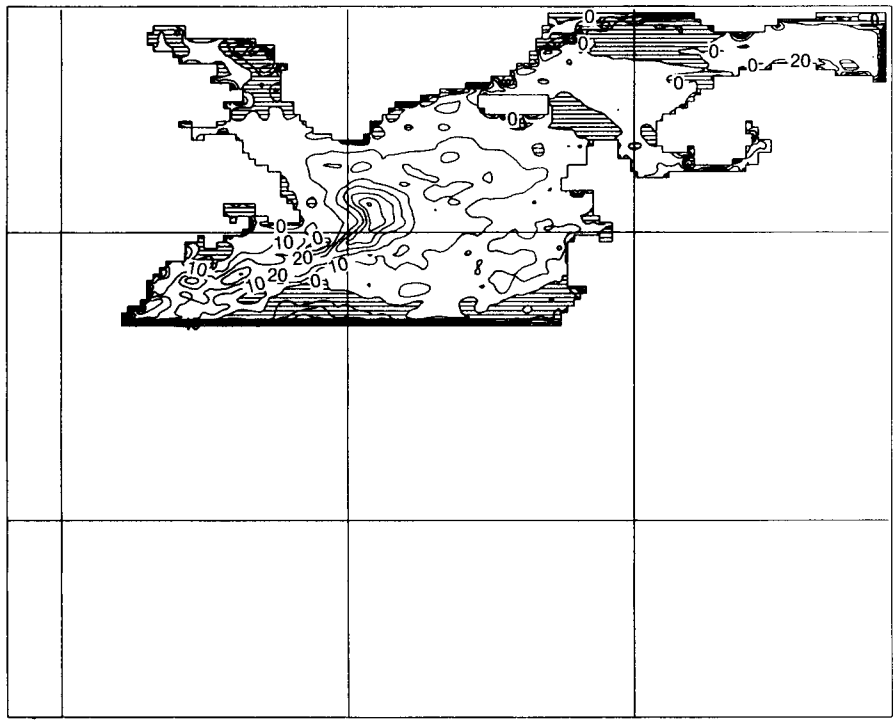

Figure 2. Difference in the monthly mean latent heat flux between the fine-and coarse-mesh models for October 1989. Contours every 10 W m^{-2} with negative areas shaded.

heat flux used for the NWP run less that used for the climatological control run. In the tropical and mid-latitude North Atlantic the NWP model has a generally larger heat flux, up to 100 W m^{-2} away from the Gulf Stream region and up to 200 W m^{-2} in the Gulf Stream area, when compared with the climatology. As already mentioned the higher resolution SST field used by the NWP models produces a larger and more localized heat flux in the Gulf Stream area.

The monthly mean difference in the SST between the NWP heat-flux-driven model and the climatological heat-flux-driven model is shown in Fig. 7. Away from the Gulf Stream region, areas of upwelling and areas of strong near-surface currents, the monthly mean difference in SST (ΔT) between the two runs is related to the monthly mean difference in the heat flux (ΔQ) through the heat equation

$$\Delta Q \simeq 2\rho c_p h \Delta T / \Delta t \qquad (3)$$

where ρ is the sea water density, c_p is the specific heat capacity of water, Δt is the period considered (one month), h is the average of the mean mixed layer depth of the two runs and $2\rho c_p / \Delta t \approx 3.1$. The factor of two in equation (3) arises as a result of using the difference in the monthly mean SST (ΔT) rather than the difference in the SST at the end of the integrations. As an example, applying equation (3) to the area on the Greenwich meridian just south of the equator where the heat flux difference (ΔQ) between the two runs is 50 W m^{-2} yields a monthly mean difference in the SST (ΔT) of approximately 1 °C ($h = 20$ m, see Fig. 8(a)) which agrees well with that shown in Fig. 7.

Equation (3) shows the dependence of the change in the ocean mixed-layer temperature on the mixed-layer depth when there is net heating or cooling of the ocean surface. Generally the mixed layer (Fig. 8(a)) is shallowest in the tropical latitudes (as shallow as 10 m or so in the October climatology of Fig. 8(a)) and increases towards the poles. In the high-latitude North Atlantic the mixed layer depth exceeds 100 m in the climatology for October. The mixed layer depth is usually deeper in mid winter, and in the North Atlantic it can reach depths of several hundred metres during extreme weather conditions.

A positive heat flux into the ocean heats the upper layers and therefore increases the stability. This leads to a reduction in the mixed layer depth which in turn leads to an increase in the sensitivity of the mixed layer temperature to the heat flux. On the other hand, when there is a net cooling, the deepening of the mixed layer through convective mixing decreases the sensitivity of the mixed layer to the heat fluxes. Fig. 8(b) shows the difference in the monthly mean mixed layer depth between the two runs. Generally, where there is more net heating in the NWP-forced run than in the climatology-forced run there is a relative reduction in the mixed layer depth, and vice versa. In the Gulf Stream area the cooling difference of 200 W m^{-2} introduces a relative deepening of the mixed layer by 10 m (15%). In the tropics, where the mixed layer is much shallower, a cooling difference of 50 W m^{-2} between the two runs introduces a relative increase in the mixed layer depth of 10 m (50% deeper). Heating of the sea surface, such as that east of Florida of 50 W m^{-2}, introduces no significant changes in the mixed layer depth, whereas

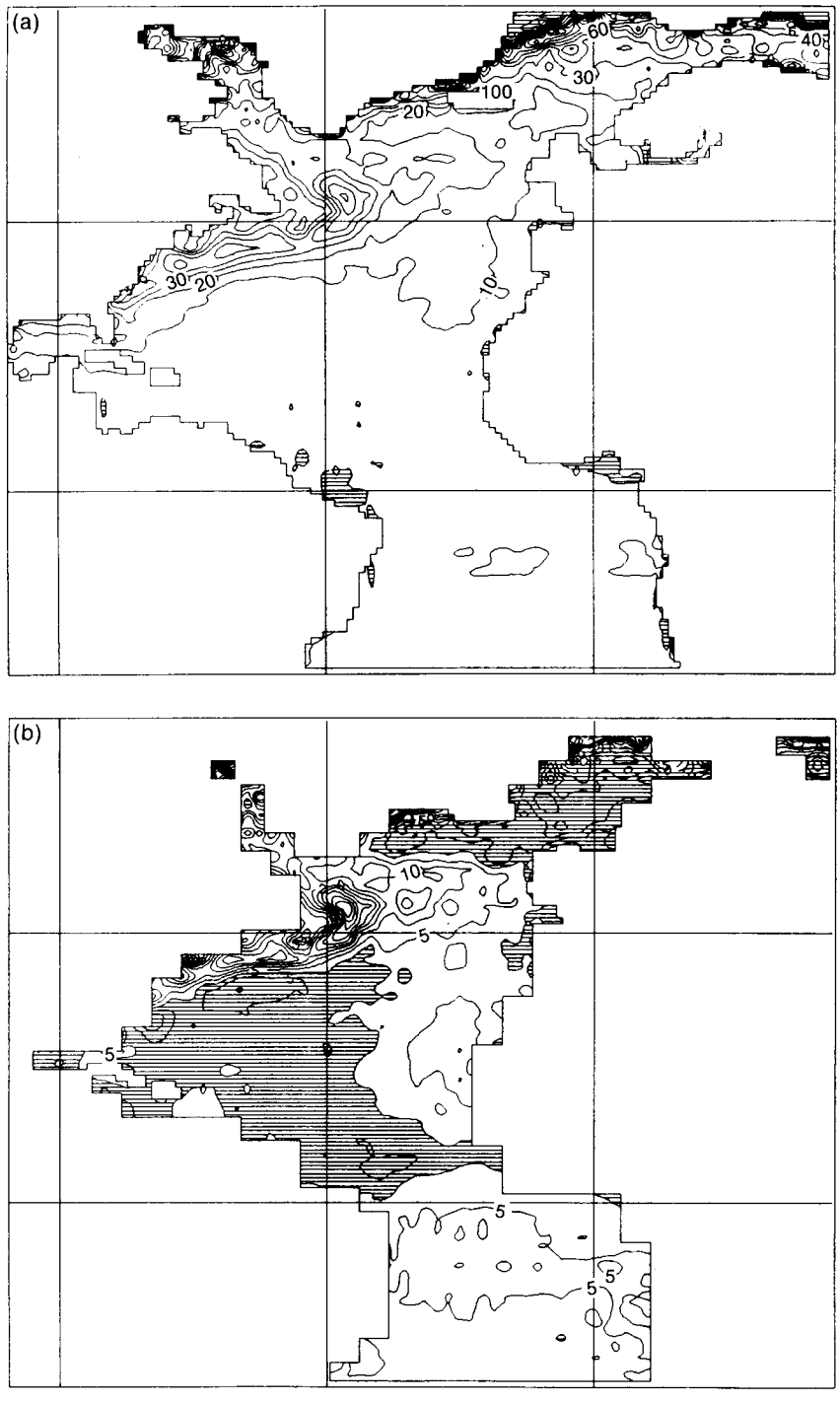

Figure 3. (a) Coarse-mesh monthly mean sensible heat flux for October 1989. Contours every 10 W m^{-2} with negative areas shaded. (b) Difference between the monthly mean sensible heat flux from the coarse-mesh model and climatology. Contours every 5 W m^{-2} with negative areas shaded.

heating differences of less than 50 W m^{-2} in the equatorial ocean, where the mixed layer is shallower, introduces differences in the mixed layer of up to 50% (for example, a shallowing of 15 m where the mixed layer depth in the climatology was 30 m).

Changes in the mixed layer depth will introduce changes in the surface current by changing the depth to which wind stress is applied via the Ekman drift mechanism. The climatology-forced model's current field for October and the vector difference from the NWP-forced models' top-layer current is shown in Fig. 9. The main differences are in the tropics where the largest changes in the mixed layer depth occur. Near the equator, differences of up to 10 cm s^{-1} occur in a region where the surface current is only 20 cm s^{-1}. The complex nature of the ocean–atmosphere system has been demonstrated here, where differences in the heat fluxes between the ocean and atmosphere not only change the ocean mixed layer temperature, but also its vertical stability and current structure.

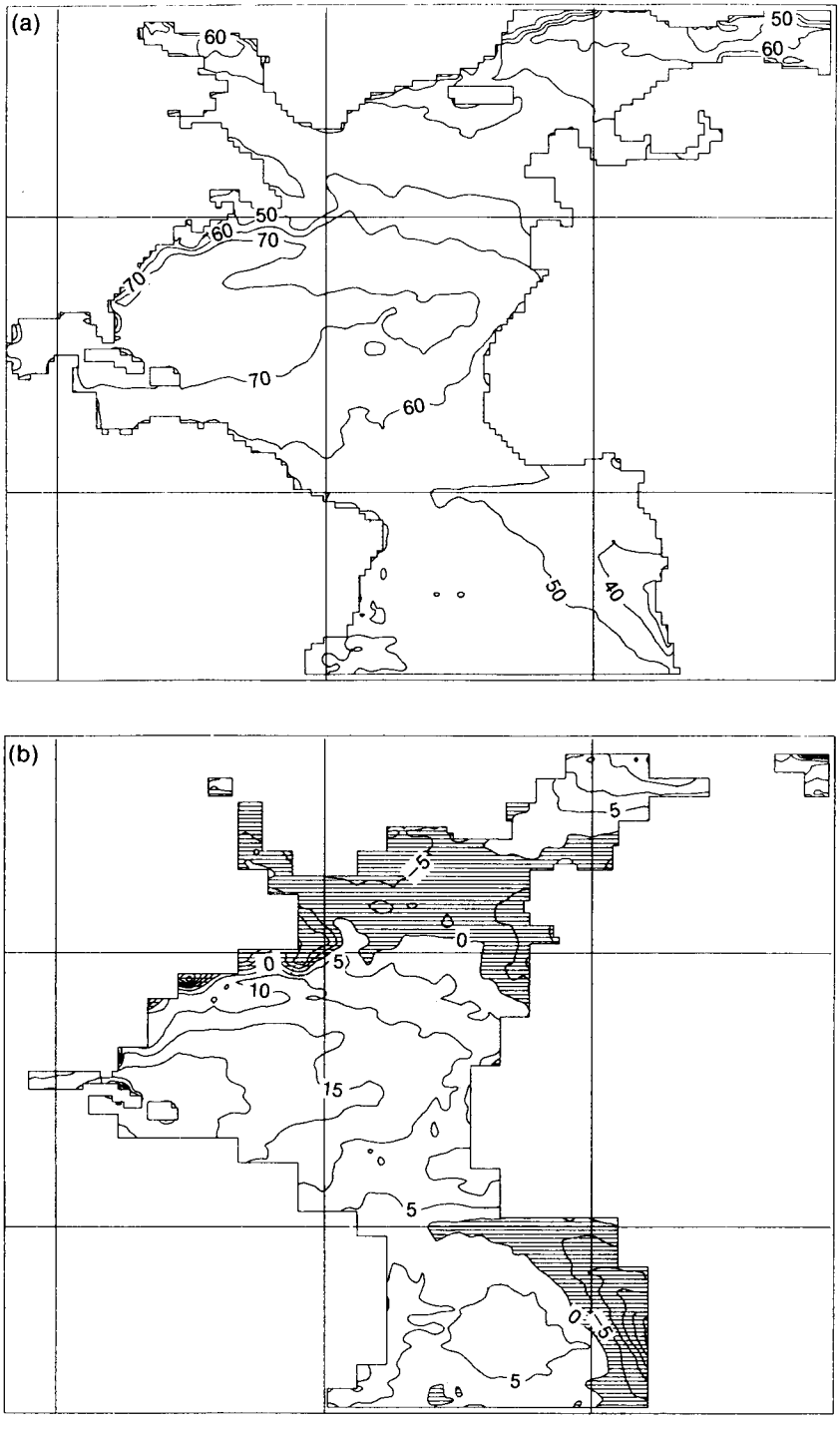

Figure 4. (a) Coarse-mesh monthly mean infrared radiation for October 1989. Contours every 10 W m^{-2}. (b) Difference between the monthly mean infrared radiation from the coarse-mesh model and climatology. Contours every 5 W m^{-2} with negative areas shaded.

4.2 Discussion

The infrared radiation depends on the distribution of cloud. In the CM model, where a zonally averaged climatological cloud distribution is used, the only zonal variability in the IR flux arises due to changes in the SST. In the FM model the cloud distribution is calculated from the humidity field. The proper assimilation of humidity data into NWP models and its representation throughout the forecast is therefore essential for determining the IR flux.

The IR flux (I) from the sea surface (assumed to be a black body) depends on the SST through the Stefan–Boltzman law

$$I = \sigma T^4$$

where σ is Stefan's constant (5.67×10^{-8} W m^{-2} K^{-4}) and T is the absolute temperature. Alves (1990) reported uncertainties of several degrees Celsius in the SST fields used by the NWP models. The uncertainty in the IR field

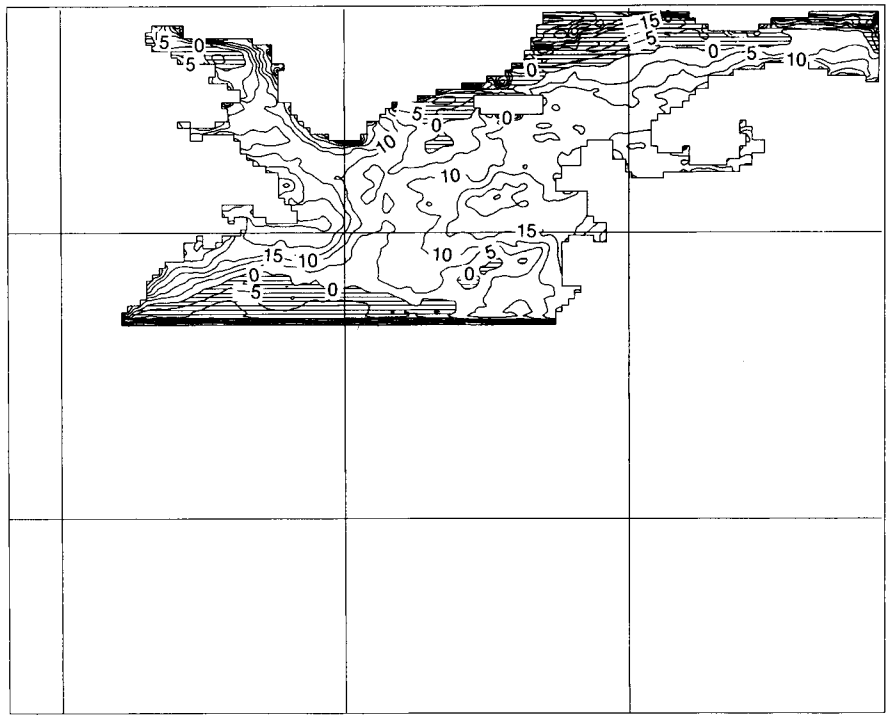

Figure 5. Differences in the monthly mean infrared radiation between the fine- and coarse-mesh models for October 1989. Contours every 5 W m^{-2} with negative areas shaded.

(ΔI) corresponding to an uncertainty in the SST (ΔT) is given by.

$$\Delta T = 4\sigma T^3 \Delta T.$$

An error in the SST of around 2 °C would result in an error in the IR flux of around 10 W m^{-2}, that is 12% to 35% of the values shown in Fig. 4(a), although the value of the IR flux is in general small when compared with the latent heat flux.

Bulk aerodynamic parametrization of the latent and sensible heat fluxes (equations (1) and (2)) makes them directly proportional to the wind speed, ignoring any dependence of the exchange coefficients on wind speed. Alves (1991) compared the FM and CM 10 m winds and an uncertainty of 10% was found. This leads to an uncertainty of 10% in each of the sensible and latent heat fluxes. For the sensible heat flux this could be a few W m^{-2} and as much as 30 W m^{-2} for the latent heat flux in the Gulf Stream region. This uncertainty in the latent heat flux is small when compared with the differences which existed between the NWP heat flux and the climatology discussed earlier.

Sensible heat flux is also directly proportional to the sea–air temperature difference and the latent heat flux is directly proportional to the sea–air humidity difference. The difference in temperature between the SST and the first sigma-level temperature is shown in Fig. 10(a) for the FM model (this was not available for the CM model). The climatological sea–air temperature difference used by Esbensen and Kushnir (1981) in their flux calculations is shown in Fig. 10(b). The climatological sea–air temperature difference is generally positive except in parts of the southern tropics, indicating a general transfer of heat from the ocean to the atmosphere. Largest differences occur along the east coast of North America, Greenland and Iceland where cold air blowing from the continents suddenly passes over a warmer ocean. Differences are also large where air blows across ocean thermal fronts such as the Gulf Stream where the maximum difference resolved in the climatology is 2.5 °C. For the FM model the temperature difference shows the same pattern as the climatology but the values are much larger. In the Gulf Stream area the difference reaches over 5 °C. This would imply a heat flux which would be twice that of the climatology (for the same wind speed and exchange coefficient). The area east of Greenland where cold polar air flows over warmer oceans contains sea–air temperature differences in excess of 7 °C. The reason for this larger value compared to the climatological value of 2.5 °C is because the NWP models use a finer resolution SST, which additionally takes account of ice, compared to the climatology.

Most of the *in situ* observations of the ocean SST are based on the 'bucket' method which involves measuring the temperature of the water collected using a bucket or measuring the temperature of water from engine intake. This water will have originated up to several metres below the ocean surface and in conditions of light winds and strong radiation it may be several degrees cooler than the top few millimetres (skin) of the ocean surface. Liu *et al.* (1979) discuss the difference obtained by using the bulk SST and the 'skin' temperature. They devise a scheme for calculating the skin temperature from the bulk temperature.

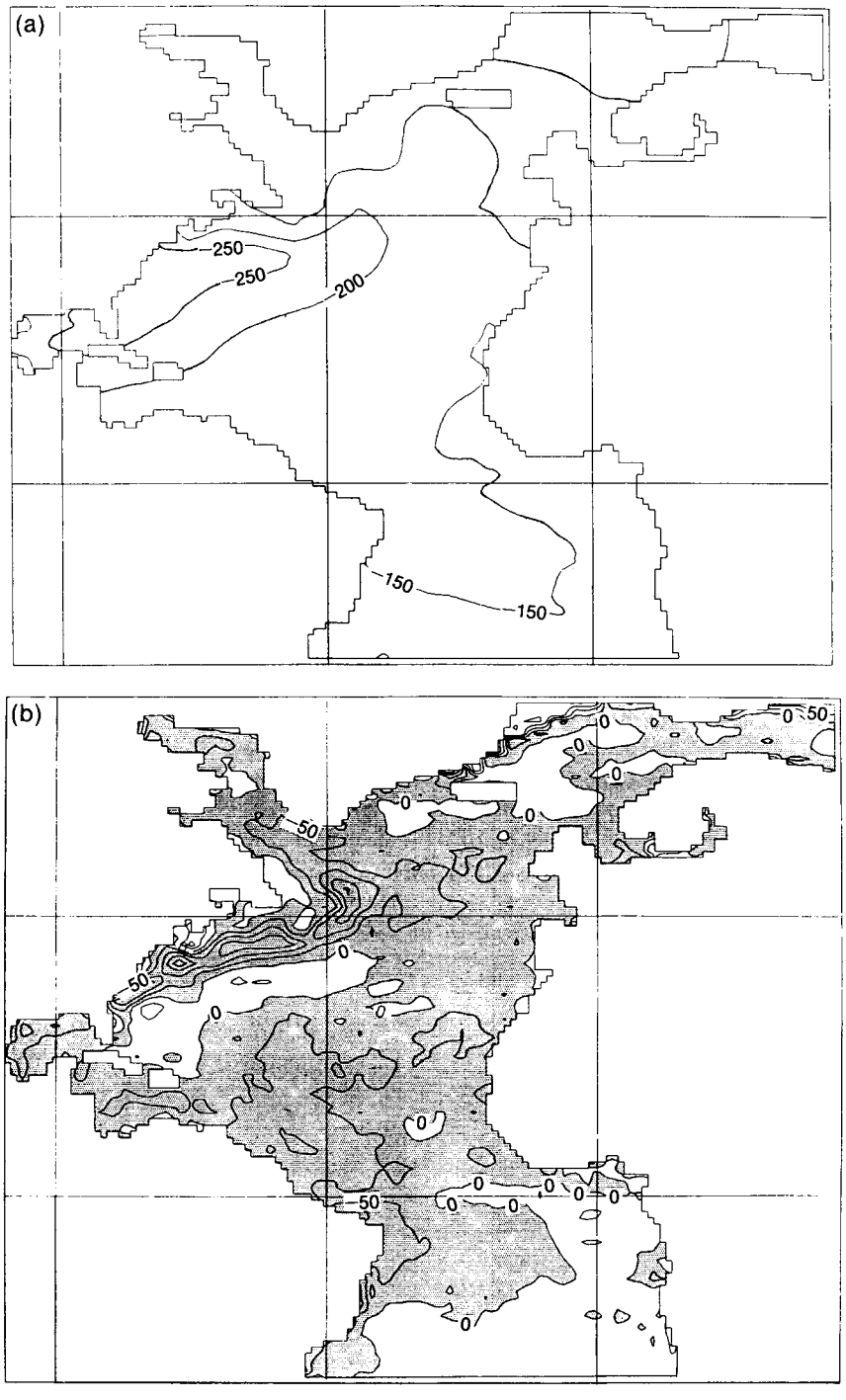

Figure 6. (a) Monthly mean climatological non-penetrative net heat flux for October. Contours every 50 W m^{-2}. (b) Difference between the monthly mean non-penetrative net heat flux between the merged NWP fields and climatology for October 1989. Contours every 50 W m^{-2} with negative areas shaded.

The present data analysis system of the MO does not use near-surface air temperature observations over the sea. This means that the first sigma-level temperature arises as a result of the surface fluxes and it will therefore alter with the SST. Since the first sigma-level temperature responds to the SST it can be argued that a bias in the SST may not seriously effect the temperature difference since the first sigma-level temperature will adjust to that bias through the heat fluxes. What may be important in producing the correct sea–air temperature difference is the correct representation of the SST gradients. This is observed in the Gulf Stream where the sea–air temperature maxima occur across the Gulf stream thermal gradients. This has already been discussed in the results where the SST field used by Esbensen and Kushnir to calculate the climatological fluxes was of a much lower resolution than that used by the NWP models, leading to a larger magnitude and

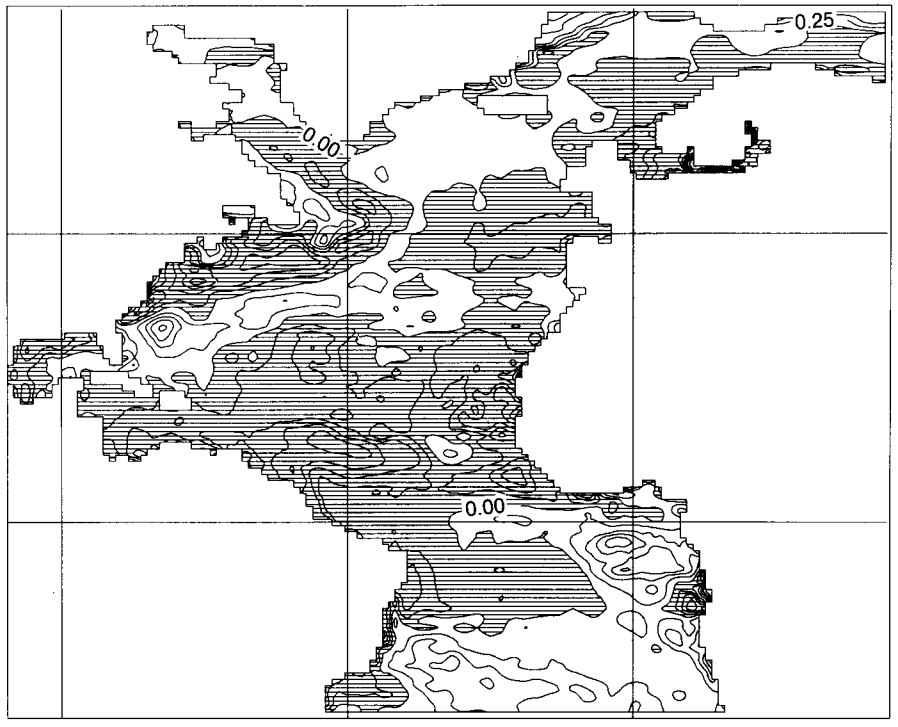

Figure 7. SST monthly mean difference between the NWP net non-penetrative heat-flux-forced run and the climatology-forced run. Contours every 0.25 °C with negative areas shaded.

more localized sensible heat flux in the NWP models. It is therefore essential to represent SST gradients accurately in the SST fields used by the NWP models.

Climatological sea–air specific humidity difference used by Esbensen and Kushnir (1981) is shown in Fig. 11(b). This increases towards the equator and the western North Atlantic. Maxima of just over 6 g kg^{-1} are found in the Gulf Stream area in the West Atlantic. The only humidity field available from the NWP models' archive was the relative humidity (H_1) at the first sigma-level for the FM model. The specific humidity was calculated from this using

$$q_1 = q_{s1} H_1$$

where the saturated specific humidity was calculated using the integrated Clausius–Clapeyron equation

$$q_{s1}(T) = q_{so}(T_o)\exp(\epsilon L/R(1/T_o - 1/T)) \qquad (4)$$

where $\epsilon = 0.622$, L is the latent heat of vaporization (2.5×106 J kg^{-1}), R is the gas constant for dry air (287 J kg^{-1} K^{-1}), $T_o = 273$ K and $q_{so} = 3.8$ g kg^{-1}. The surface humidity $q_s(T_*)$ was also calculated using the Clausius–Clapeyron equation (4). Resulting sea–air humidity differences are shown in Fig. 11(a). The pattern is similar to that of the climatology but is less smooth, partly as a result of a higher resolution SST. The maximum in the Gulf Stream area reaches up to 10 g kg^{-1}, which would give a latent heat flux 66% larger than the climatological one (for the same wind speed and exchange coefficient). Dependence of the saturated surface humidity on the SST introduces the same problems which arise in the calculation of the sensible heat flux. These are the requirement to accurately represent thermal gradients in the ocean surface; use of the 'bucket' temperature as the sea surface temperature; and the need to reduce biases in the SST field used by the NWP models. The last of these may be less critical since the first sigma-level humidity field, like the temperature field, does not contain any assimilated data. It will therefore adjust through the latent heat flux to the surface value calculated from the prescribed SST.

In both FM and CM models the exchange coefficients for heat and moisture are made equal. Further, under stable conditions the exchange coefficients are equal to the drag coefficient. Fig. 12 shows the dependence of C_H on wind speed for various stabilities (ΔT) for the CM and FM models. Both models' C_H parametrizations agree well for wind speeds in the range 5–8 m s^{-1}. For wind speeds greater than 7 m s^{-1} there is little stability dependence of the values of C_H used by both models. The CM uses a constant value for the neutral C_H of 1.2×10^{-3} whereas the FM value increases with wind speed as a result of using the Charnock formula to parametrize the surface roughness length. The same problem occurs as for the drag coefficient (since for stable conditions $C_D = C_H = C_E$, see Alves (1991)), for example, for a wind speed of 20 m s^{-1} the FM uses a value for C_H of 2.1×10^{-3}, nearly twice that used by the CM. For low wind speeds and during stable or slightly unstable conditions, differences between the two models' C_H arise due to the Charnock formula used in the FM model decreasing the neutral value of C_H to zero

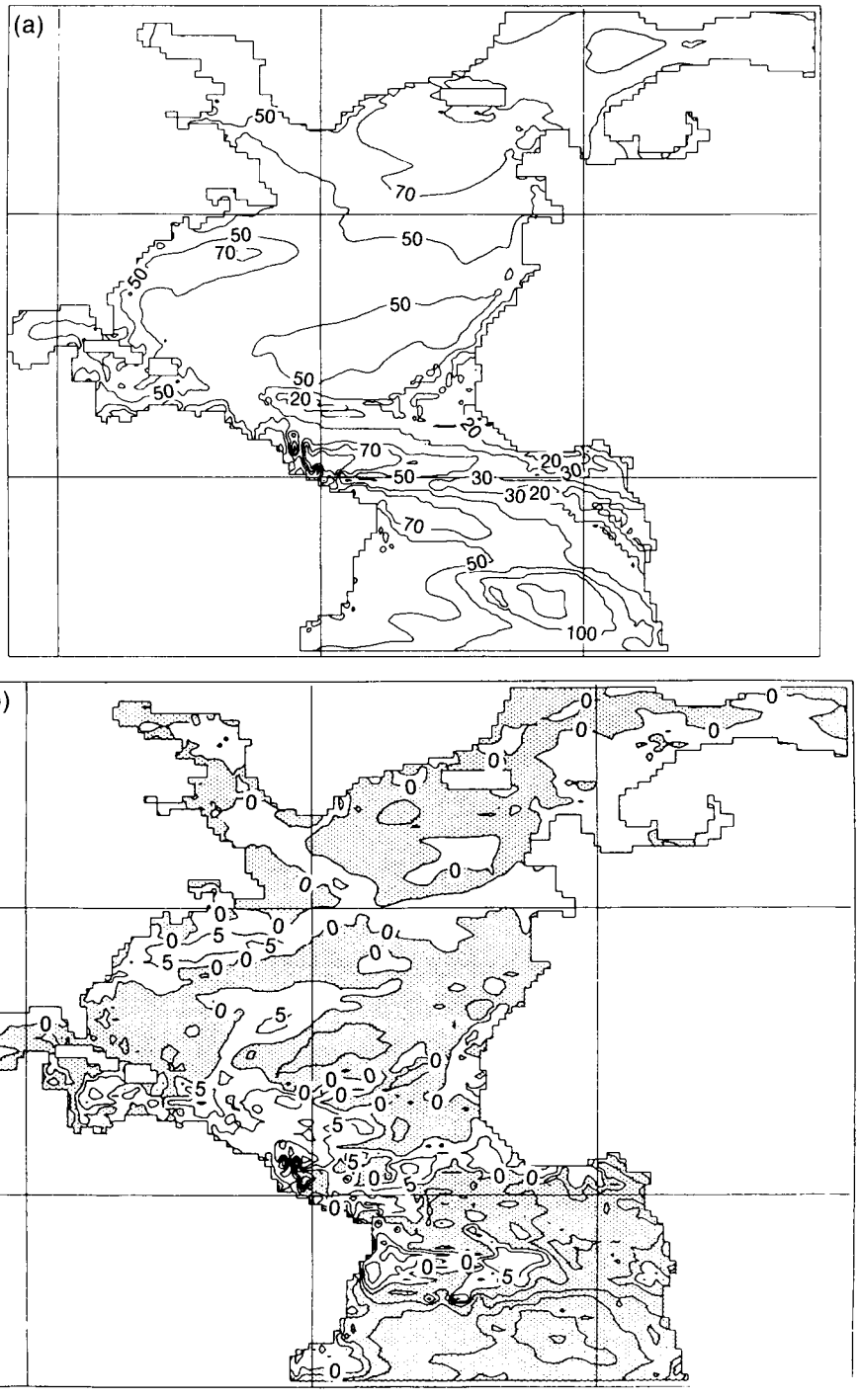

Figure 8. (a) Monthly mean mixed-layer depth produced by the climatological run. Contours at 10, 20, 30, 50, 70, 100, 150 and 200 m. (b) Difference in the monthly mixed-layer depth between the NWP non-penetrative heat flux run and the climatological run. Contours every 5 m with negative areas shaded.

with the wind speed, whereas the CM uses a constant value for the neutral C_H. Under highly unstable conditions, such as that of free convection (Ri_B less than -100), the values used by the two models differ greatly. The values shown on each chart for the lowest wind speed is that when free convection arises. The FM predicts a value of 2×10^{-3}, whereas the CM uses a value of 12.1×10^{-3}, six times greater (Ri_B of -100).

Blanc (1985) compared the empirical formulae for C_H and C_E of several authors under neutral or slightly unstable conditions. Plots for these are shown in Fig. 13. Most of the authors have taken $C_H \approx C_E$ as is indeed done in the FM and CM models. For moderate wind speeds, in the range 3–10 m s^{-1} the agreement between the authors is at its best with the maximum difference being 0.5×10^{-3}, i.e. 50%. The average value in this range for both C_E and C_H is 1.2×10^{-3}, which is in good agreement with the CM and FM models in the range 5–8 m s^{-1}. For stronger winds Masagutov (1981) and Bunker (1976) indicate a wind speed dependence with

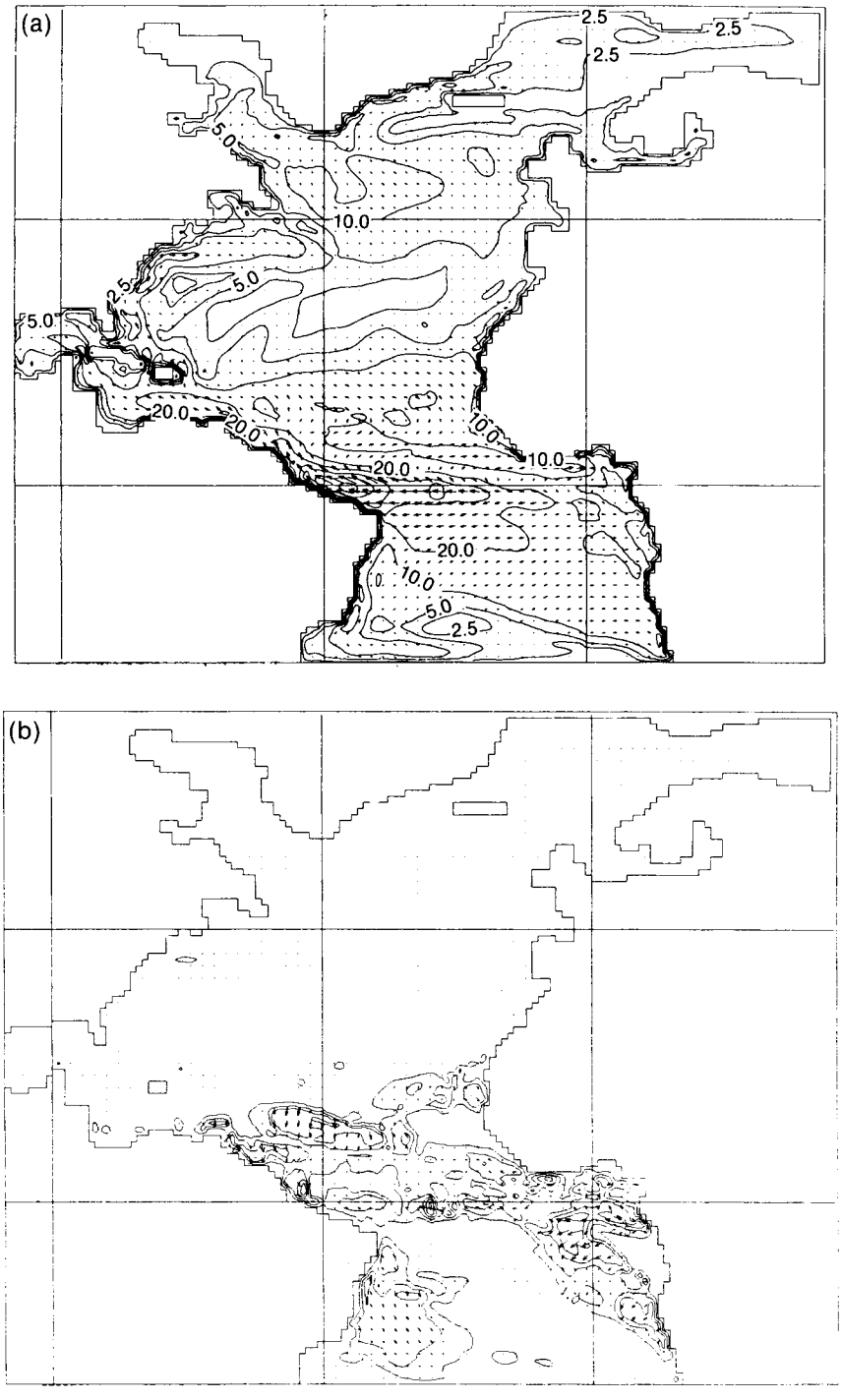

Figure 9. (a) Monthly mean model top-level current vector field produced by the climatological run for October. Contours at 2.5, 5, 10, 20, 40, 60 and 100 cm s^{-1}. (b) Difference in the model top-layer current field between the NWP non-penetrative heat flux run and the climatological run. Contours at 1, 2.5, 5, 10 and 20 cm s^{-1}.

C_H and C_E increasing with wind speed. At 20 m s^{-1} their schemes average to give $C_H = C_E = 1.7 \times 10^{-3}$, 40% larger than the CM value of 1.2×10^{-3} and 20% less than the FM value of 2.1×10^{-3}. Other authors (see Fig. 13) predict neutral C_E and C_H which have little or no wind speed dependence. Their average value is about 1.15×10^{-3} for both C_E and C_H which is in good agreement with the value used by the CM and for a wind speed of 20 m s^{-1} it is 45% less than the FM value. For low wind speeds the neutral C_H is estimated by the various authors to either remain constant or increase slightly, having an average value of about 1.2×10^{-3}. This agrees well with the CM model but disagrees with the FM model where the Charnock formula used to parametrize the surface roughness makes the values of C_H and C_E tend to zero with the wind speed.

Liu *et al.* (1979) devise a model which uses the surface 'skin' temperature, calculated from the 'bulk' sea surface temperature to calculate values for C_H and C_E. Their results indicate that for strong winds both C_E and C_H

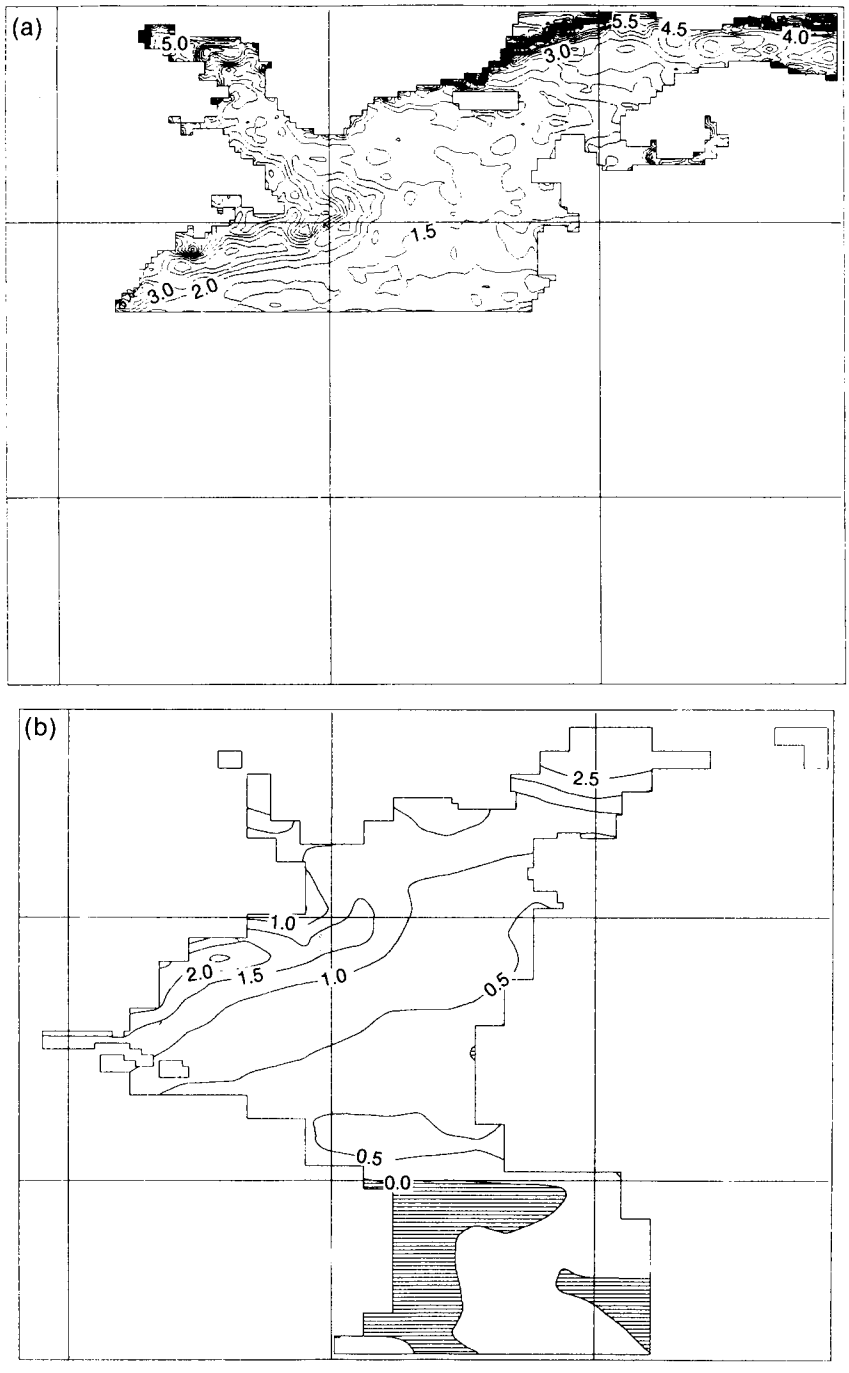

Figure 10. Monthly mean air–sea temperature difference (a) from the fine-mesh model for October 1989, and (b) that used by Esbensen and Kushnir (1981). Contours at 0.5 °C intervals.

decrease slightly with increasing wind speed. Large and Pond (1982) argue that the neutral values for C_H increase with wind speed for unstable conditions but remain constant for stable conditions. Data used by them are shown in Fig. 14 for C_H as a function of stability and wind speed and C_E as a function of wind speed. There is a clear indication of a different behaviour in the value of C_H for stable and unstable conditions. Their results show that for stable conditions the value for the neutral C_H is a constant, 0.7×10^{-3}, much lower than either the FM or CM models. For unstable conditions the neutral value of C_H is 1.1×10^{-3} for wind speeds less than 10 m s^{-1} and increases linearly with wind speed for stronger values, the value for C_H at a wind speed of 20 m s^{-1} being 1.3×10^{-3}. This indicates a wind speed dependence much less than that when the Charnock formula is used for the roughness length. Large and Pond (1982) suggest that the neutral C_E should have a constant value of 1.15×10^{-3} for wind speeds less than 10 m s^{-1}, in good agreement with the CM and the FM in the wind speed range 5–8 m s^{-1}. For stronger winds the linear wind speed dependence is such

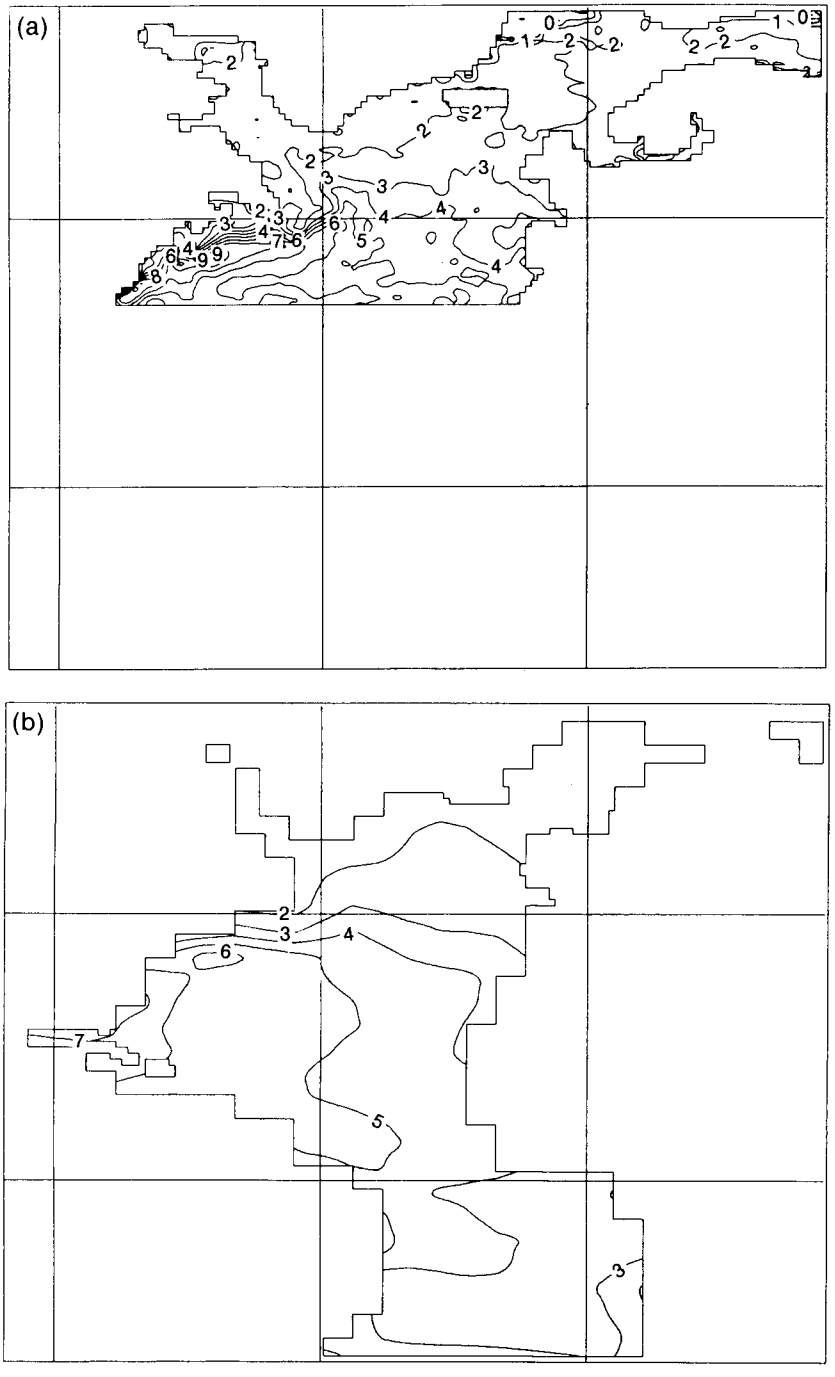

Figure 11. Monthly mean air–sea specific humidity difference (a) from the fine-mesh model for October 1989, and (b) that used by Esbensen and Kushnir (1981). Contours every 1 g kg^{-1}.

that C_E is 1.3×10^{-3} for a wind speed of 14 m s^{-1}. The FM value for a wind speed of 14 m s^{-1} is 1.7×10^{-3}, clearly indicating a much stronger wind dependence.

Under extremely unstable conditions, and conditions of free convection, the values of C_H and C_E become large for the CM model. For the FM model, where the same similarity function is used, the values for C_H and C_E are much less as a result of a smaller surface roughness length. Clearly the Charnock formula is inappropriate at low wind speeds when such conditions occur. Gordon and Hunt (1989) discuss the similarity scheme used for free convection by the CM model, and compare it with other schemes. They conclude that the CM scheme predicts a latent heat flux some 25 W m^{-2} less than the other schemes and suggest some amendments to the present scheme.

The experimental results shown in Fig. 14 show a large scatter and this explains the many differences in the formulations of the various authors considered by Blanc (1985). There is no clear evidence as yet to suggest the dependence on stability or wind speed, if any, of either values of C_H and C_E. The dependence of the drag

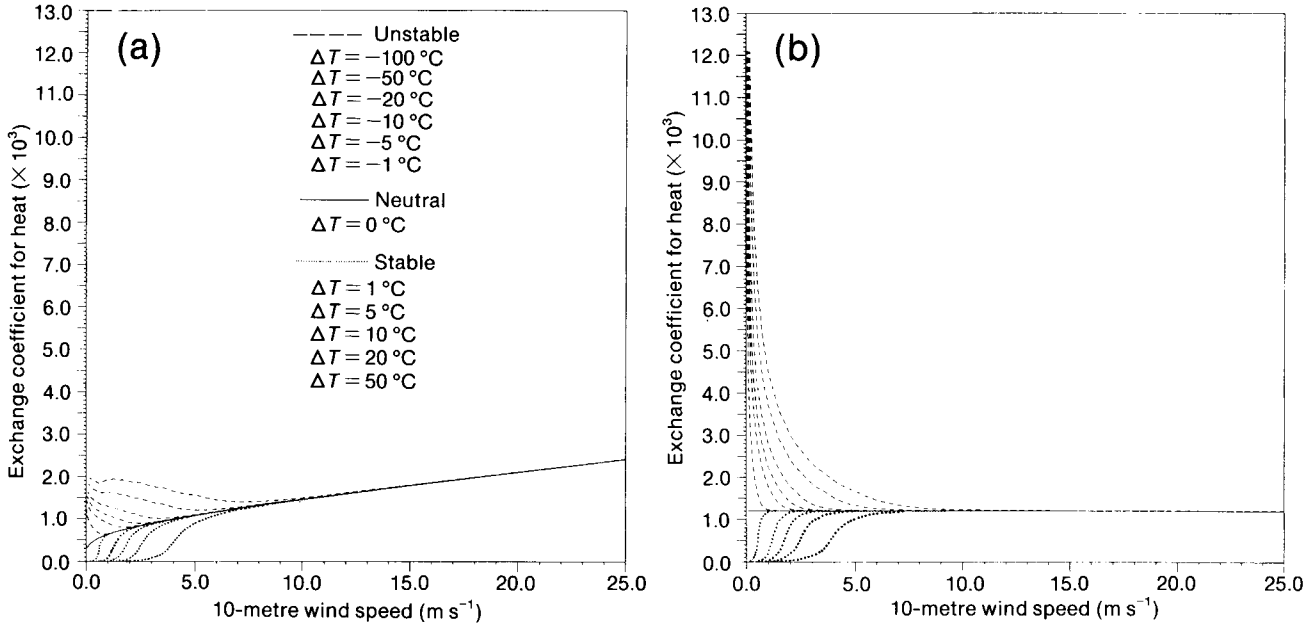

Figure 12. Exchange coefficient for sensible heat as a function of wind speed for various air–sea temperature differences and zero humidity difference for (a) the fine-mesh and (b) the coarse-mesh models.

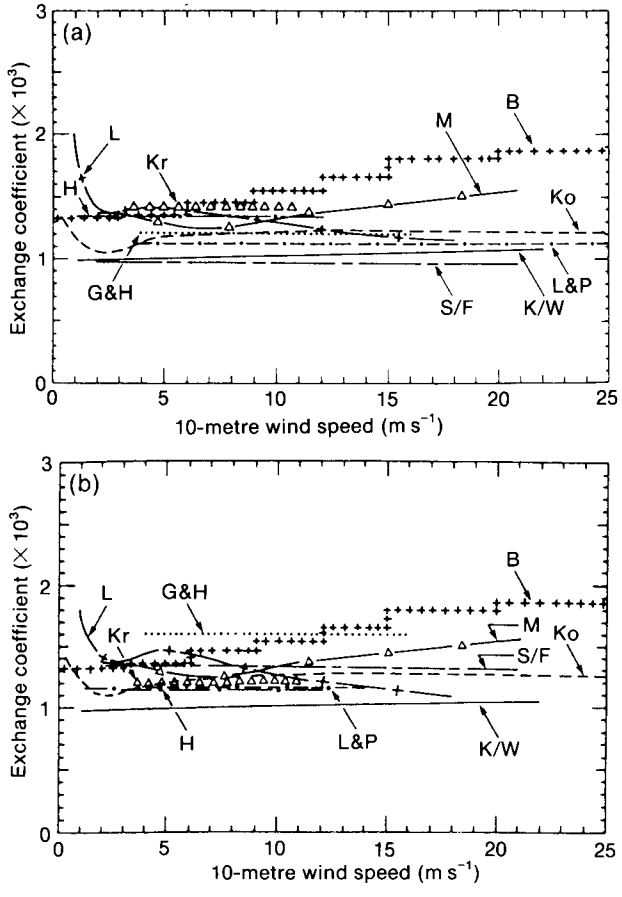

Figure 13. The neutral or slightly unstable exchange coefficients for (a) sensible heat and (b) latent heat as a function of the 10 m wind (from Blanc (1985)). Sources are: K/W = Kitaygorodskiy *et al.* (1973) and Wu (1980); Ko = Kondo (1975); G&H = Garratt (1977) and Garratt and Hyson (1975); B = Bunker (1976); Kr = Krügermeyer (1976); S/F = Smith (1980) and Friehe and Smith (1976); H = Hasse *et al.* (1978); L = Liu *et al.* (1979); M = Masagutov (1981); L&P = Large and Pond (1981, 1982).

coefficient on sea state (discussed by Alves (1991)) would suggest that C_H and C_E may also depend on sea state to some extent. Even so, it is clear that the present formulation used by the FM overestimates the values of C_H and C_E for strong winds and underestimates them for light winds. The CM has a better representation even though it has no wind dependence.

5. Solar heat flux

5.1 Results

The main problem with the solar heat flux is that the CM model uses a cloud distribution which is essentially a zonally averaged climatology. This is apparent in Fig. 15(a) which shows the merged mean solar heat flux for October 1989 used to drive the ocean model. Outside the FM region there is little zonal variation. Fig. 15(b) shows the NWP merged solar heating for October 1989 less a climatological field (Esbensen and Kushnir 1981). The 'bull's-eye' of 130 W m^{-2} (50% more than the climatological value) in the southern tropical ocean clearly indicates that such a zonally averaged radiation could not realistically be used to drive an ocean model. Furthermore, in the NWP model most of the tropical Atlantic has a much larger solar heat flux than climatology, with the departure from climatology increasing as one moves south-eastwards across the equator.

In the FM region the interactive cloud scheme gives a field which varies both meridionally and zonally. When compared with the climatology (Fig. 15(b)) the FM field is generally some 10–50 W m^{-2} (up to 40% of total) higher throughout most of the mid-latitude North Atlantic.

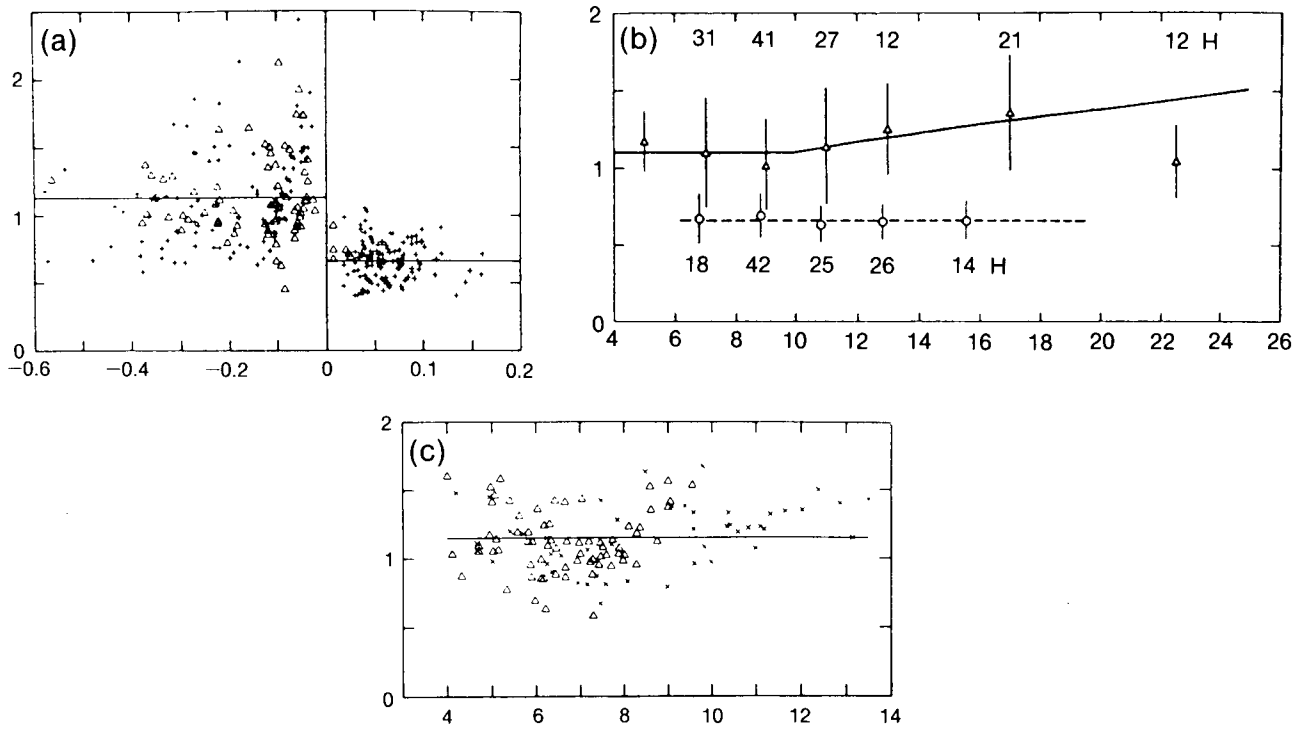

Figure 14. Experimental plots of the exchange coefficient for (a) sensible heat as a function of stability, (b) as a function of the 10 m wind speed (m s^{-1}) and (c) the exchange coefficient for latent heat as a function of the 10 m wind speed (m s^{-1}) (from Large and Pond (1982)).

Fig. 16 shows the difference in the ocean model's top-level temperature between the solar and climatology runs. A monthly mean SST warming of over 1.8 °C occurs in the region where the 'bull's-eye' (Fig. 15) was located and extends down to a depth of around 30 m (not shown). In the FM region there is also a general monthly mean warming of up to 0.6 °C (corresponding to solar flux difference of 50 W m^{-2}). Solar heating leads to an increase of the stratification in the upper layers of the ocean and therefore a decrease in the mixed layer depth (for constant wind mixing energy). A decrease in the mixed layer depth will increase the sensitivity of the SST to solar heating. The hypothesized decrease in the mixed layer depth due to solar heating can be confirmed in Fig. 17. The 'bull's-eye' heating in Fig. 17 resulted in a reduction in the mean mixed layer depth for that month of around 140 m (over 75% of initial value) and in the FM area the maximum heating difference of 50 W m^{-2} reduces the monthly mean mixed layer depth by around 5 m (about 10% of initial value).

Reduction in the mixed layer depth due to solar heating decreases the depth of water to which the momentum flux from the atmosphere is applied directly through the Ekman drift mechanism. This will, of course, change the structure of the currents in the upper layers of the ocean. Fig. 18 shows the monthly mean vector difference between the solar and climatology runs' model top-layer current field. Large solar radiation differences in the tropical Atlantic introduce relatively large anomalous currents throughout the region. The difference in the magnitude of the currents between the two runs is comparable with the magnitudes of the currents themselves. These are also comparable to differences between model integrations using NWP wind stress and climatological wind stress (see Alves (1991)). In the FM region there are no significant differences in the near surface currents mainly due to much deeper mixed layers. Throughout the Atlantic there is no significant difference between the currents of the two runs below the mixed layer.

5.2 Discussion

The calculation of the solar heat flux is mainly sensitive to two factors, the representation of cloud and surface albedo. Derivation of cloud amount (outlined in section 2) depends upon the model humidity field. In the NWP data-analysis scheme used by the MO only humidity measurements from conventional soundings of the atmosphere are used. Sparseness of these soundings over the ocean and the difficulty in measuring humidity render the humidity fields used by the NWP models to be of poor quality. This is an area which requires a great effort in improving the observations of humidity and their assimilation into NWP models. Inability to represent cloud correctly in NWP models will remain the main source of error in the solar heat flux at the surface.

The value α_o (0.06 in the FM model) is the value for the sea surface albedo used under clear sky conditions (it is modified for multiple reflection when clouds are present). This value is know to vary with the elevation of the sun and the sea state. The amount of reflection from the sea surface is known to increase as the sun's elevation decreases. Representing this effect may be important to

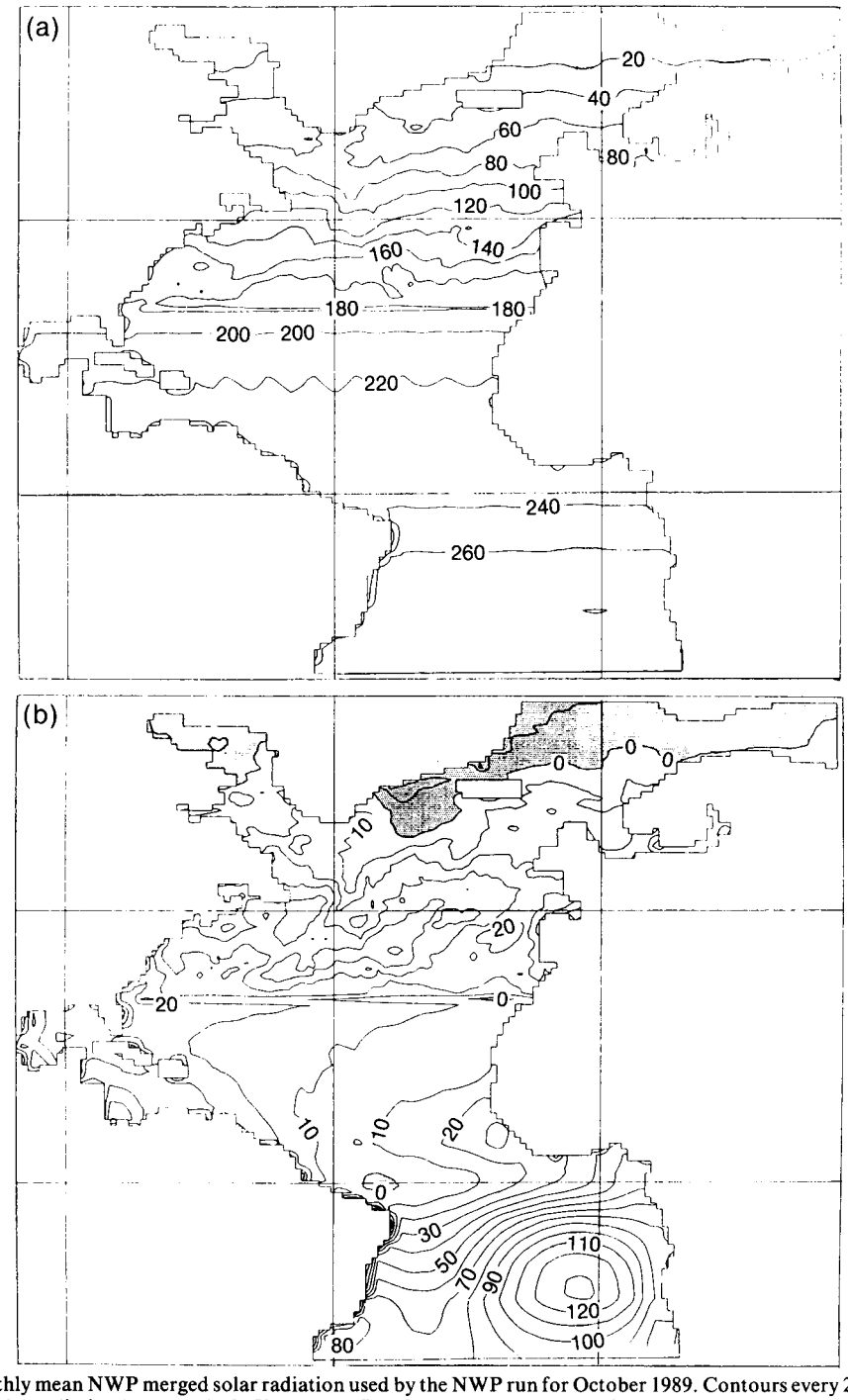

Figure 15. (a) Monthly mean NWP merged solar radiation used by the NWP run for October 1989. Contours every 20 W m^{-2}. (b) Difference in the monthly mean solar radiation between the NWP merged field for October 1989 and climatology. Contours every 20 W m^{-2} with negative areas shaded.

model the daily cycle of the oceanic mixed layer.

Dependence of the surface albedo on the sea state becomes important during periods of strong winds. The formation of whitecaps (foamy mixture of water and air produced by breaking waves) increases the surface albedo since the whitecaps themselves are believed to have an albedo of about 0.5 (Stabeno and Monahan 1986). Spillane *et al.* (1986) show maps of monthly mean whitecap distribution. The maximum whitecap coverage occurs during winter in the North Atlantic and covers about 4% of the ocean. Taking the albedo of the whitecap-free sea surface to be 0.06, the surface albedo under the maximum whitecapping conditions above would be 0.08 (30% greater). It must be emphasized that this is the maximum influence of whitecapping on the surface albedo and it would only be of importance under strong winds and clear skies.

Even where there are no breaking waves, for increasing roughness of the sea, the albedo increases for small zenith angles (near 0°) and decreases for large zenith angles (near 90°) (Nunez *et al.* 1972). The opacity of the water also effects the surface albedo with the albedo increasing with a decrease in transparency (Kondratyev 1972).

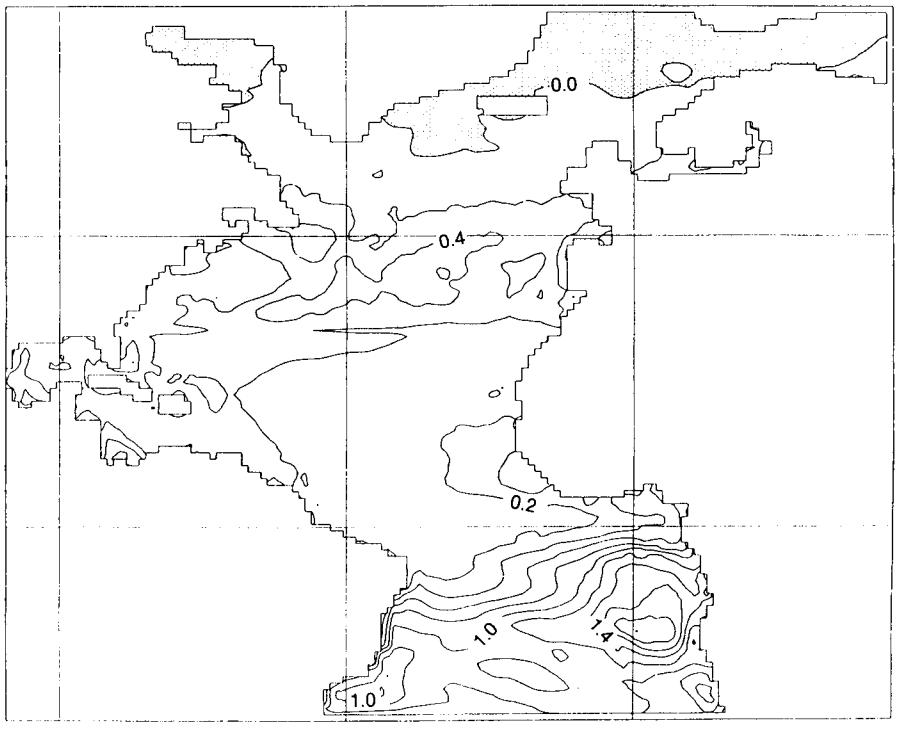

Figure 16. Monthly mean SST difference between the NWP solar run and the climatological run. Contours every 0.2 °C with negative areas shaded.

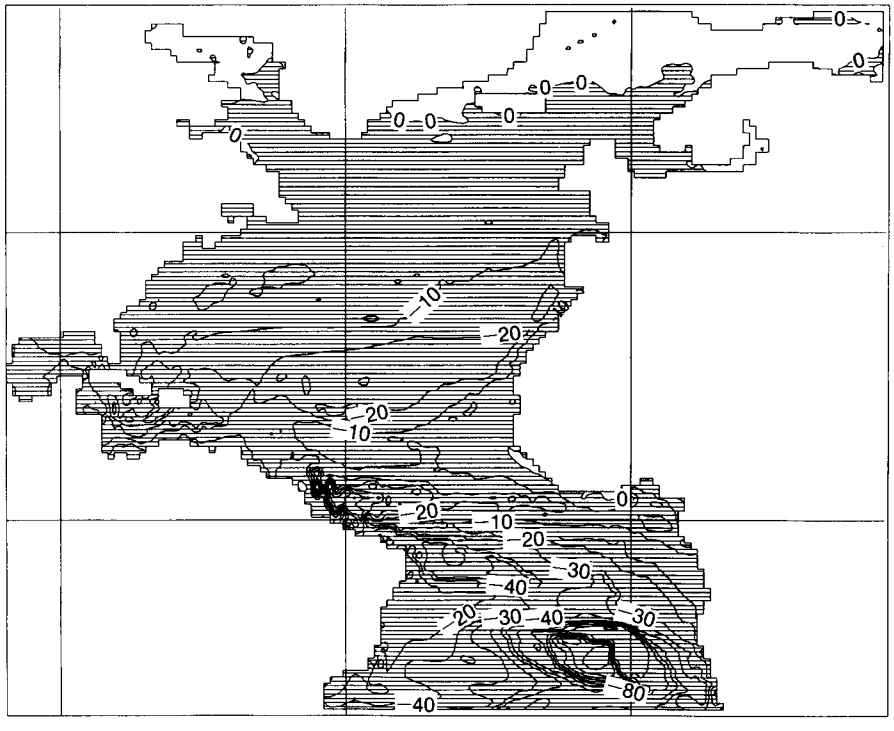

Figure 17. Monthly mean difference in the mixed-layer depth between the solar NWP run and the climatological run. Contours every 10 m with negative areas shaded.

6. Fresh water flux

6.1 Results

The PME (Precipitation Minus Evaporation) field gives a value for the net fresh water flux into the ocean from the atmosphere. Fig. 19(a) shows the climatological PME field for October (precipitation is due to Jaeger (1983) and evaporation is from Esbensen and Kushnir (1981)). Generally evaporation exceeds precipitation except for the region of the ITCZ (Inter Tropical Convergence Zone) in the east tropical North Atlantic, parts of the Caribbean and in the latitude range 50° N–60° N. A region of excess rainfall associated with the ITCZ is concentrated off the west coast of Africa from

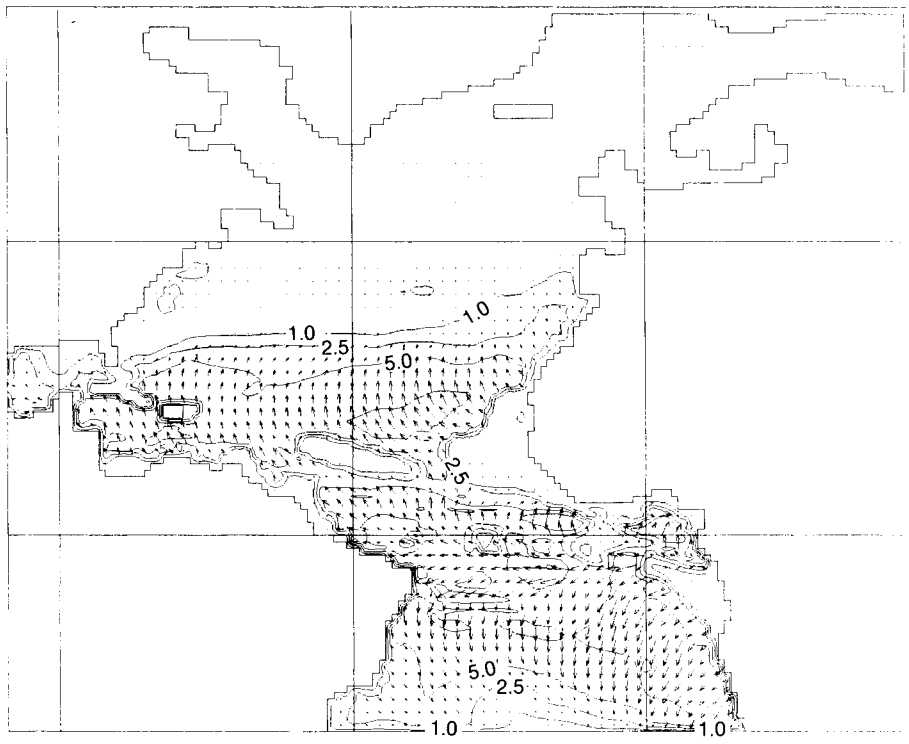

Figure 18. Monthly mean vector difference in the surface current between the solar NWP run and the climatological run. Contours at 1, 2.5, 5, 10 and 20 cm s^{-1}.

around 10°S to 15°N, with the PME reaching 7.5 mm day^{-1}. Fig. 19(b) shows the merged PME field from the NWP models. The ITCZ is represented by a narrower band of larger PME extending from the equator to about 10°N in the east Atlantic. Excess of precipitation over evaporation extends into the west tropical Atlantic, along the Brazilian coast and into the South Caribbean. In the east Atlantic it reaches values of up to 10 mm day^{-1} in the region of the climatological ITCZ and in the west Atlantic it reaches 5 mm day^{-1} in a region where the climatological value is of the opposite sign. Clearly the NWP PME has a stronger ITCZ which spreads out over a longer band across the tropical Atlantic. Confirmation of this actually happening has not been sought.

The difference between the two PME fields is plotted in Fig. 20(a). It emphasizes the large PME in the CM model in the north-western tropical Atlantic which is up to 7.5 mm day^{-1} greater than the climatology. In the west Atlantic, between the latitudes 15°N and 45°N where the climatology shows a negative PME of about 2.5 mm day^{-1}, the NWP model produces much less evaporation and/or much more precipitation, with the PME reaching a positive value of 5 mm day^{-1} in the central part of this region. North of about 45°N the agreement between the two is generally to within 2.5 mm day^{-1} which is of the same magnitude as the PME value.

Temperature and salinity of the ocean affect the ocean circulation by changing the density structure. The PME field, where positive, decreases the salinity of the mixed layer (and vice versa where negative). To establish the importance of a change in salinity on the ocean circulation we need to quantify its relative effect on density. Gill (1982) gives a standard formula relating the density of sea water to the temperature and salinity. Linearizing that formula it can be deduced that the change in density due to a change in temperature ΔT is equivalent to a change in salinity ΔS (in parts per thousand (ppt)) given by

$$\Delta S \simeq \frac{(-0.08-0.02T)}{(0.9-0.004T)}\Delta T$$

where the temperature T is in °C. Taking $\Delta T = 1$ °C, then for the tropics (with $T = 25$ °C) we obtain, that for a similar change in density, it would require $\Delta S = -0.7$ ppt. For the polar regions taking $T = 0$ °C then $\Delta S = -0.09$, nearly an order of magnitude less than in the tropics. This clearly shows that salinity differences due to the PME field will be of greater relative importance in the higher latitudes where the temperature of the mixed layer is cooler.

Differences between the two models top-level monthly mean salinity field are shown in Fig. 20(b). The large difference in the PME field in the region of the ITCZ introduces differences in the salinity field of up to 0.25 ppt, this having a similar effect on the density as a temperature difference of about 0.3 °C which is not significant when compared to the differences produced by the heat fluxes. North of about 45°N differences in the salinity field is generally less than 0.05 ppt, this being equivalent to a temperature change of around 0.5 °C. Therefore a PME difference of 2.5 mm day^{-1} in the polar regions has a similar effect on the upper-ocean density

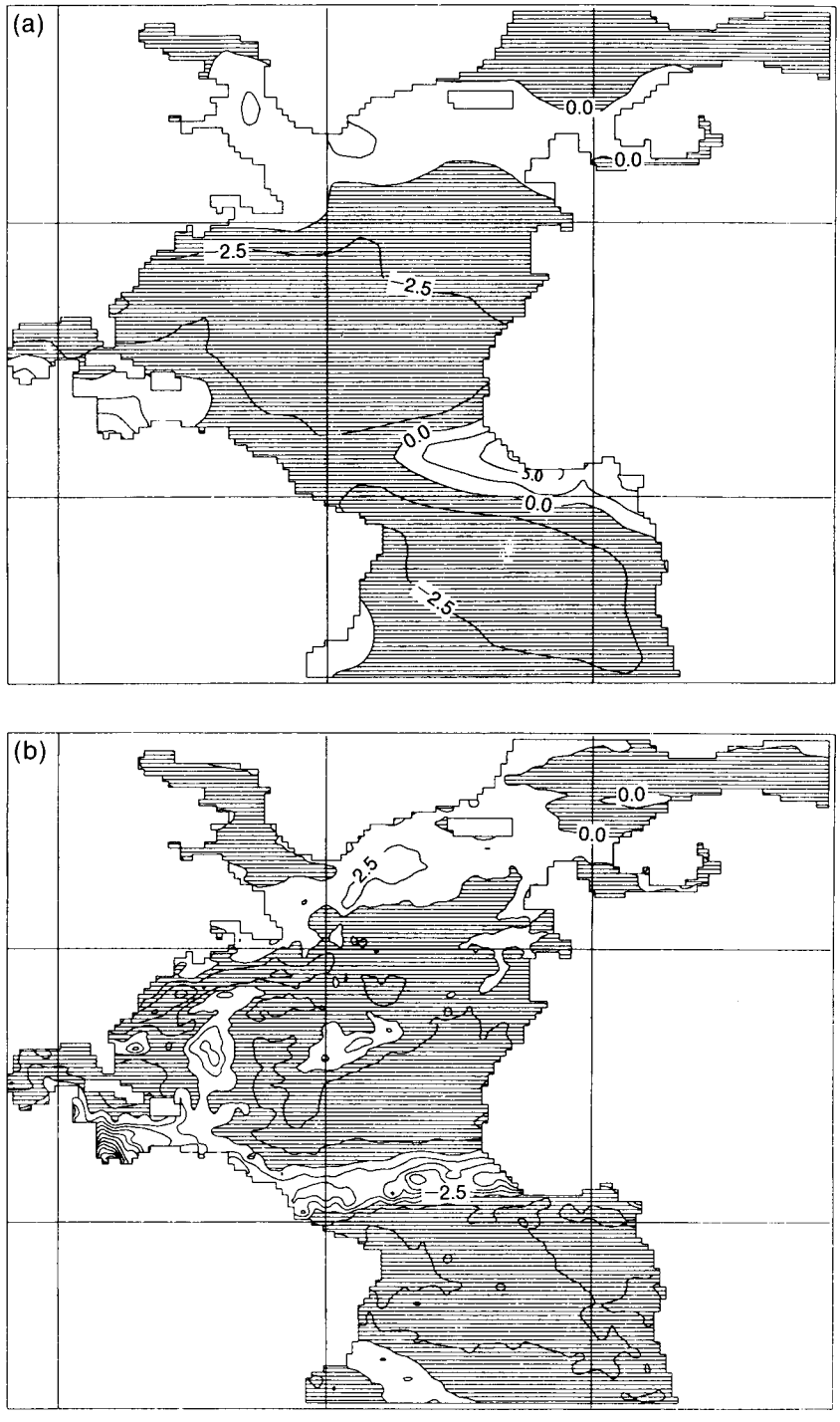

Figure 19. Monthly mean precipitation minus evaporation for (a) climatology and (b) merged NWP field for October 1989. Contours every 2.5 mm day^{-1}.

field as a PME difference of around 10 mm day^{-1} in the tropics.

Fig. 21 shows the difference in the mixed layer depth between the two runs. Where the NWP has excess water flux into the ocean, the increase in buoyancy of the surface water leads to a reduction in the mixed layer depth of up to 30 m in the tropics (on average a 50% reduction). The PME is less than that of the climatology in the Gulf of Guinea and the mixed layer depth there is increased by around 15 m from a monthly mean depth of 25 m. Although these changes in the mixed layer depth do not significantly affect surface temperature (not shown) it does introduce differences in the current field (Fig. 22). Vector differences of over 5 cm s^{-1} occur in a region of the tropics where the surface current is around 20 cm s^{-1}, these differences being restricted to the mixed layer. Away from the region of the ITCZ there are no significant differences in the current field.

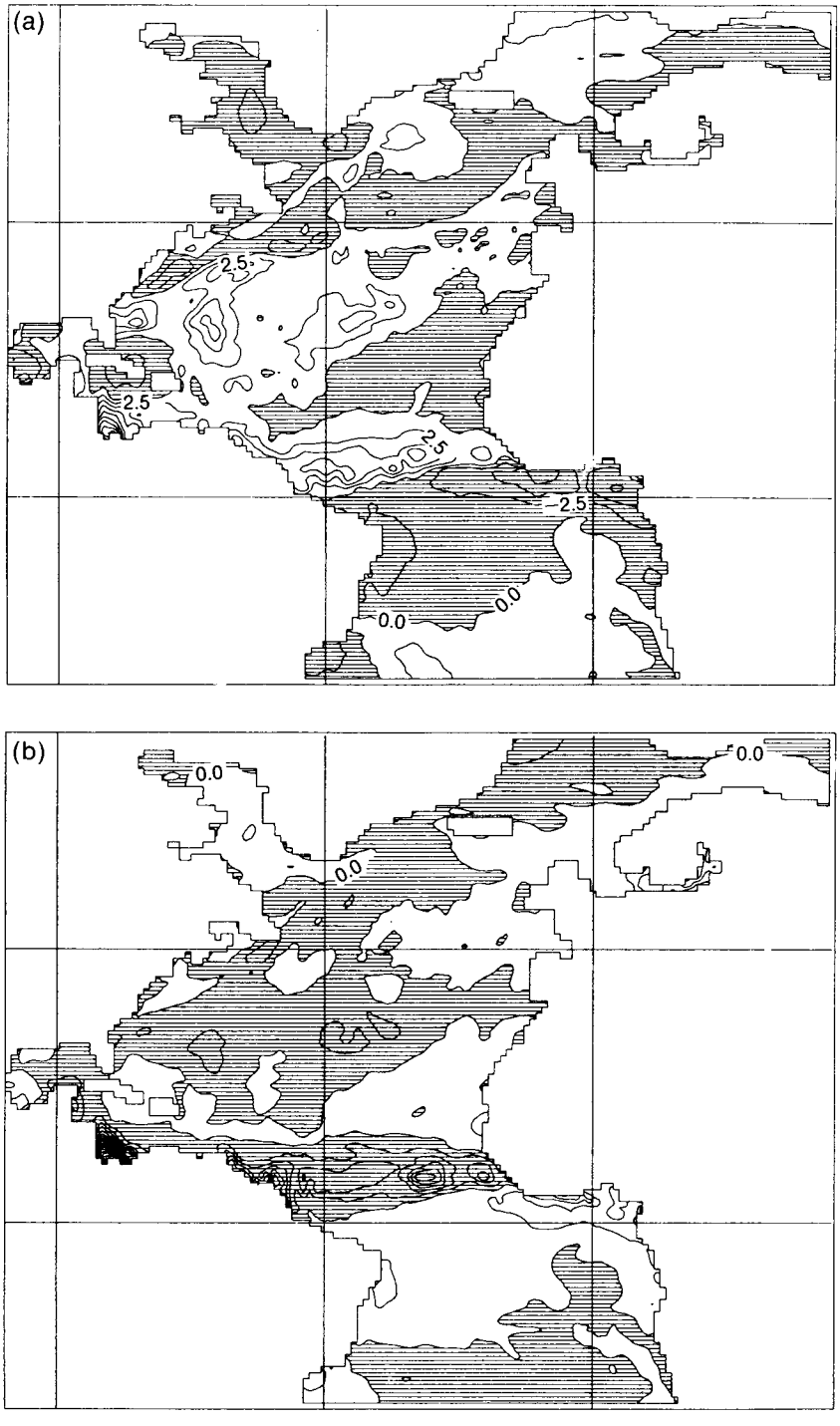

Figure 20. (a) Difference between monthly mean NWP merged and climatology PME fields. Contours every 2.5 mm day^{-1} with negative areas shaded. (b) Monthly mean difference in the top-layer salinity field between the NWP PME integration and the climatological one. Contours every 0.05 ppt with negative areas shaded.

6.2 Discussion

The parametrization of the evaporation flux has already been discussed as the latent heat flux in section 5. The precipitation depends critically upon the humidity field, therefore emphasizing the need to improve the assimilation of humidity data and its representation in NWP models.

Differences in the NWP models' PME field were shown to be more important in areas where the SST was lowest due to the dependence of the density on salinity. However, because of the shallower mixed layers in the warmer SST regions of the tropics, significant differences in the current field were observed. In general, differences were small when compared with the differences due to the heat, solar and momentum fluxes. The specification of the PME field is therefore secondary to that of the other surface fluxes.

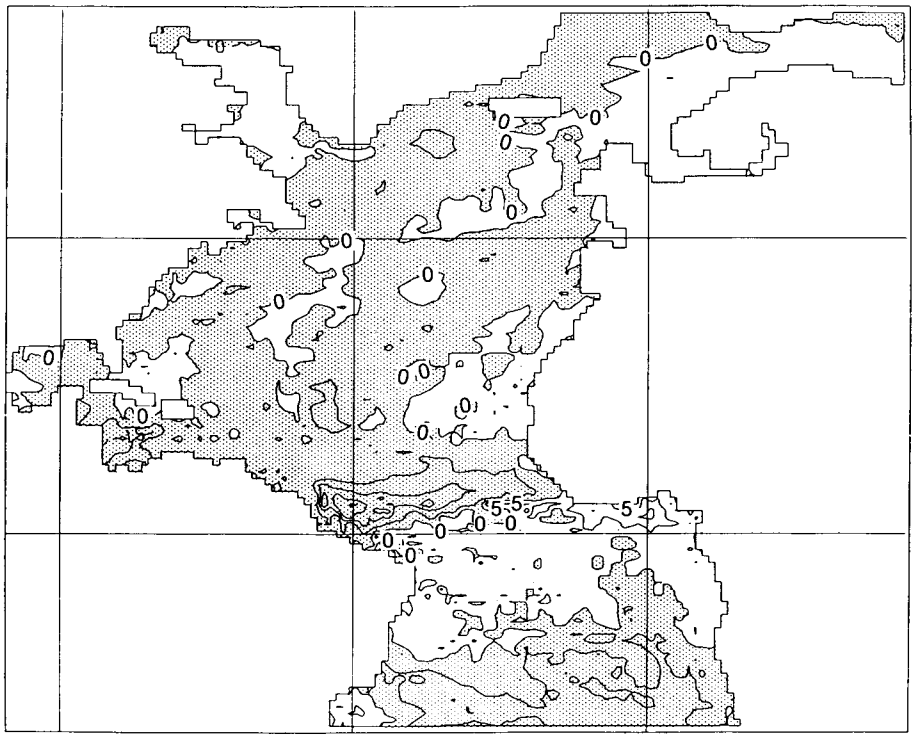

Figure 21. Monthly mean difference in the mixed-layer depth between the NWP PME and climatology runs. Contours every 5 m with negative areas shaded.

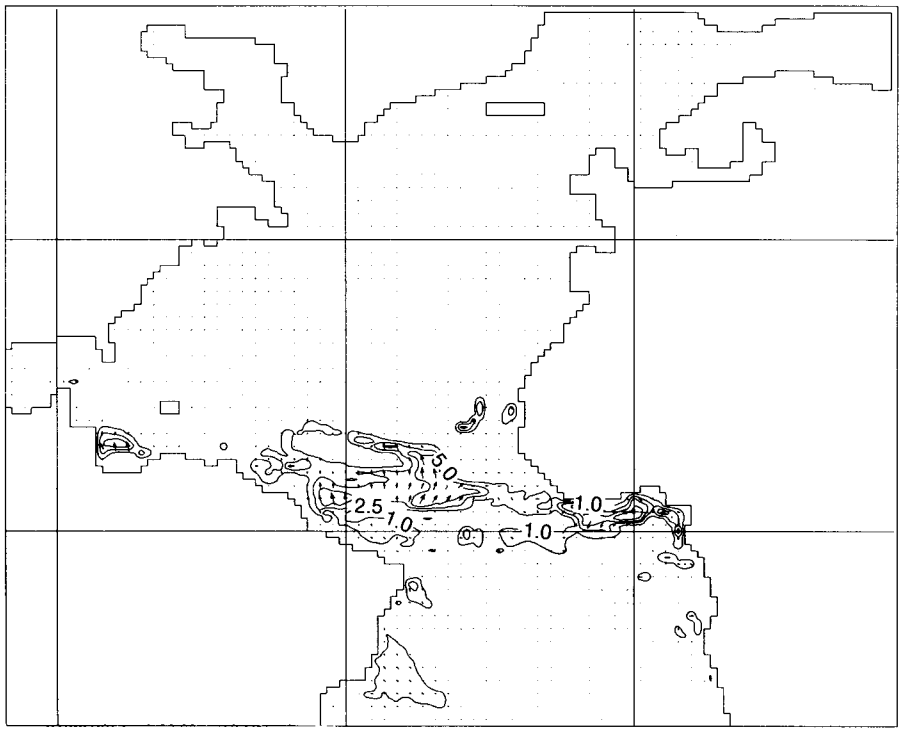

Figure 22. Monthly mean vector differences in the model top-layer current between the NWP PME and climatology runs. Contours at 1, 2.5, 5 and 10 cm s^{-1}.

7. Summary, conclusion and recommendations

7.1 Non-penetrative heat fluxes

The IR flux ranges from 30 to 80 W m^{-2} throughout the North Atlantic. Differences of up to 50% from the monthly mean climatology were noted for the CM model. In the tropical North Atlantic the CM IR flux was some 50% or so greater than the climatology. Comparison of the FM and CM models' IR flux revealed differences of up to 25 W m^{-2}, representing a percentage difference of 50%, this being partly due to the use of a zonally averaged climatological cloud distribution in the CM model. The strong dependence of the IR

flux on cloud emphasizes the need to improve the assimilation of humidity into NWP models and its representation throughout the forecast. Possible errors in the SST field used by the NWP models were reported and an uncertainty of 1 °C in the SST field would yield uncertainties in the IR flux of up to 17% in the equatorial Atlantic. This uncertainty represents typically 5 W m^{-2} which is relatively small when compared to uncertainties in the latent heat flux.

In the Gulf Stream area, where the maximum sensible heat flux occurred, the CM predicted values for the sensible heat flux which were 65% or so greater than the climatological values. The FM increased this difference by a further 15%. The 10% uncertainty in the wind speed, due to differences between the FM and CM 10 m winds, leads to uncertainties of 10% in the sensible heat flux. More important, a strong dependence of the sensible heat flux on the SST gradient was shown, with the NWP models producing a more localized and larger magnitude heat flux across the Gulf Stream than the climatology which used a SST field of lower resolution. This emphasizes the need to use high resolution SST fields as the lower boundary condition for the NWP models. The air–sea temperature difference was shown to contribute significantly to the differences between the NWP and the climatological values of the sensible heat flux. Since, over the sea, temperature observations are not assimilated into the lowest level of the NWP model, the air–sea temperature difference is dependent on the model adjustment through the heat fluxes. Whether the assimilation of temperature into the first model level would improve the heat flux is questionable given that the SST fields used at present are known to have relatively large errors (Alves 1990). Values for the exchange coefficient for the sensible heat flux agree well for the two models and published values for wind speeds in the range 5–8 m s^{-1}. For stronger winds the published values show a large spread and there is an uncertainty as to whether there is a stability and/or wind speed dependence. The CM uses a constant value which agrees with some of the published results. The FM value increases with wind speed, due to the use of the Charnock formula to parametrize the surface roughness length, it being nearly twice that used by the CM for a wind speed of 20 m s^{-1}. The FM parametrization clearly overestimates the value of C_H when compared with other authors for strong winds. For light winds the CM keeps its constant value of 1.2×10^{-3}, agreeing with the published values, whereas the FM value decreases to zero with decreasing wind speed. The use of the Charnock formula is clearly not appropriate for light winds. Under conditions of free convection the values for C_H used by the FM model is six times less than that used by the CM model, which itself is reported to be too low (Gordon and Hunt 1989).

The latent heat flux is the dominant of the three heat fluxes (sensible, latent and IR) with its maximum value reaching over 300 W m^{-2} in the Gulf Stream area for the CM model. The monthly mean values from the CM model were up to 100 W m^{-2} (33%) greater than the climatological values. The FM values increased this difference by a further 15% or so. The higher resolution SST field used by the NWP models compared to that used to calculate the climatological heat fluxes resulted in the latent heat flux being more localized and of a larger magnitude where there was strong SST gradients, such us that of the Gulf Stream. The same 10% uncertainty is applicable to the latent heat flux due to uncertainties in the wind speed. The dependence of the latent heat flux on the specific humidity difference was shown to be of importance and this difference was much greater than the climatological value. Similar conclusions can be drawn for the latent heat flux as for the sensible heat flux, these being the need to accurately represent SST gradients and that the humidity difference arises due to the model adjustment to the specified SST through the water flux from the sea surface (constant times the latent heat flux). Again, it is not clear whether the assimilation of humidity observations into the lowest level of the NWP models would improve the latent heat flux due to known biases in the prescribed SST field. The values used for the exchange coefficient for the latent heat flux for both CM and FM models is the same as that used for the sensible heat flux. The same conclusion as for the value of C_H can be made; that there is no clear evidence as yet to suggest the dependence on stability or wind speed, if any, of either values of C_H and C_E. Even so, it is clear that the present formulation used by the FM overestimates the values of C_H and C_E for strong winds and underestimates them for light winds. The CM has a better representation even though it has no wind dependence.

The combination of the three heat fluxes above to form the net heat flux was used to force the ocean model. In general, the monthly mean net heat flux from the NWP models for October 1989 was up to 100 W m^{-2} greater than the climatology away from the Gulf Stream area and up to 200 W m^{-2} greater than the climatology in the Gulf Stream area. The latent heat flux was by far the larger of the three heat fluxes. When there was net heating of the ocean the mixed layer depth was reduced and this decreased the depth of the water column into which heat was input. Thus the sensitivity of the SST to the heat fluxes was shown to depend on the mixed layer depth, this made the tropical ocean much more sensitive to errors in the fluxes than the mid-latitude ocean.

7.2 Solar radiation flux

The solar heat flux, together with the latent heat flux, is the main contributor towards the mixed layer heat balance, with the sensible and IR fluxes, in general, having relatively smaller values. The results presented clearly show that a radiation scheme which uses cloud distribution derived from an interactive cloud scheme is essential. The radiation flux from the CM model which uses a zonally averaged climatological cloud distribution

was totally unsuitable for use in ocean model integrations. In the FM region, differences between the NWP solar flux and the climatological solar flux of up to 50 W m^{-2} produces mixed layer temperature differences of up to 0.6 °C in a region of a relatively deep mixed layer, although there was no significant difference in the current field.

The dependence of the solar flux on various physical parameters has been discussed. By far the most important is the dependence on cloud distribution. The cloud distribution is derived from the model's humidity field whose realism over the ocean is based on the assimilation of a relatively small number of conventional atmospheric soundings. Further progress in improving the quality of the surface solar flux must first be in the parametrization of cloud and the representation of humidity in the NWP models. This clearly requires a great effort in improving techniques for measuring humidity and putting them into practice routinely. The solar flux can then be further improved by taking into account the dependence of the surface albedo on the solar zenith angle and the sea state, opacity and its geometry.

7.3 Fresh water flux

The monthly mean PME field from the NWP models represents an ITCZ which extends further into the West Atlantic than the climatology and has a larger intensity. In the western tropical North Atlantic the PME field is up to 7.5 mm day^{-1} more than the climatology (the climatology is of the opposite sign, i.e. excess of evaporation over precipitation). In the middle latitudes the differences are less than 2.5 mm day^{-1}. The effect of the changes in the salinity field on the near-surface density structure, due to differences in the PME field, were shown to depend critically on the SST. The large differences in the PM field between the two runs of 7.5 mm day^{-1} in the tropics had a similar effect on the density structure as a difference of 2.5 mm day^{-1} in the high latitudes. Overall, the changes due to the differences in the PME fields were small when compared to those due to the differences in the heat, momentum and solar fluxes, although significant differences occurred in the equatorial current field as a result of shallower mixed layers.

The specification of the PME field is secondary to that of the other fluxes — momentum, heat and radiation. The evaporation rate is equivalent to the latent heat flux and its deficiencies have already been discussed in the heat fluxes above. The precipitation depends on the model's humidity field. This again emphasizes the need to represent humidity accurately in the NWP models.

References

Alves, J.O.S., 1990: A comparison of sea surface temperatures from three analysis schemes. (Unpublished, copy available from National Meteorological Library, Bracknell.)

—, 1991: An assessment of the surface fluxes from the Meteorological Office numerical weather prediction models. Part I: Momentum. *Meteorol Mag*, **120**, 200–211.

Bell, R.S. and Dickinson, A., 1987: The Meteorological Office operational numerical weather prediction system. *Sci Pap, Meteorol Off*, No. 41.

Blanc, T.V., 1985: Variation of bulk-derived surface flux, stability, and roughness results due to the use of different transfer coefficient schemes. *J Phys Oceanogr*, **15**, 650–669.

Bolton, J.A., 1981: The estimation of zonally averaged climatological cloud data for use in the 5 level model radiation scheme. (Unpublished, copy available from National Meteorological Library, Bracknell.)

Bunker, A.F., 1976: Computations of surface energy flux and annual air-sea interaction cycles of the North Atlantic Ocean. *Mon Weather Rev*, **104**, 1122–1140.

Charnock, H., 1955: Wind stress on a water surface. *Q J R Meteorol Soc*, **81**, 639–640.

Cox, M.D., 1984: A primitive equation, three dimensional model of the ocean. Princeton, Geophysical Fluid Dynamics Laboratory, Ocean Group Technical Report No. 1.

Esbensen, S.K. and Kushnir, Y., 1981: The heat budget of the global ocean: An atlas based on estimates from surface marine observations. Corvallis, Oregon State University, Report No. 29.

Friehe, C.A. and Schmitt, K.F., 1976: Parameterization of air-sea interface fluxes of sensible heat and moisture by the bulk aerodynamic formulas. *J Phys Oceanogr*, **6**, 801–809.

Garratt, J.R., 1977: Review of drag coefficients over oceans and continents. *Mon Weather Rev*, **105**, 915–929.

Garratt, J.R. and Hyson, P., 1975: Vertical fluxes of momentum, sensible heat and water vapour during the air mass transformation experiment (AMTEX) 1974. *J Meteorol Soc Jpn*, **53**, 149–160.

Gill, A.E., 1982: Atmosphere–Ocean dynamics. London, Academic Press.

Gordon, C. and Hunt, D.L., 1989: Surface evaporation during free convection. (Unpublished, copy available from National Meteorological Library, Bracknell.)

Hasse, L., Grünewald, M., Wucknitz, J., Dunckel, M. and Schriever, D., 1978: Profile derived turbulent fluxes in the surface layer under disturbed and undisturbed conditions during GATE. *'Meteor' Forschungsergebnisse*, **13**, 24–40.

Jaeger, L., 1983: Monthly and areal patterns of mean global precipitation. *In* Street-Perrott, A., Beran, M. and Ratcliffe, R. (eds), Variations in the global water budget. Dordrecht, Reidel.

Kitaygorodskiy, S.A., Kuznetsov, O.A. and Panin, G.N., 1973: Coefficients of drag, sensible heat, and evaporation in the atmosphere over the surface of the sea. *Atmos Ocean Phys*, **9**, 644–647.

Kitchen, J.E., 1986: An implicit version of the operational model boundary layer routine. (Unpublished, copy available from National Meteorological Library, Bracknell.)

Kondo, J., 1975: Air-sea bulk transfer coefficients in diabatic conditions. *Boundary Layer Meteorol*, **9**, 91–112.

Kondratyev, K.Ya., 1972: Radiation processes in the atmosphere. Geneva, WMO, No. 309.

Kraus, E.B. and Turner, J.S., 1967: A one-dimensional model of the seasonal thermocline, II. The general theory and its consequences. *Tellus*, **19**, 98–105.

Krügermeyer, L., 1976: Vertical transports of momentum, sensible and latent heat from profiles at the tropical Atlantic during ATEX. *'Meteor' Forschungsergebnisse*, **11**, 51–77.

Large, W.G. and Pond, S., 1981: Open ocean momentum flux measurements in moderate to strong winds. *J Phys Oceanogr*, **11**, 324–336.

—, 1982: Sensible and latent heat flux measurements over the ocean. *J Phys Oceanogr*, **12**, 464–482.

Liu, W.T., Katsaros, K.B. and Businger, J.A., 1979: Bulk parameterization of air-sea exchanges of heat and water vapor including the molecular constraints at the interface. *J Atmos Sci*, **36**, 1722–1735.

Masagutov, T.F., 1981: Calculation of vertical turbulent fluxes in the marine atmospheric surface layer of tropical latitudes. *Sov Meteorol and Hydrol*, No. 12, 47–53.

Nunez, M., Davies, J.A. and Robinson, P.J., 1972: Surface albedo at a tower site in lake Ontario. *Boundary Layer Meteorol*, **3**, 77–86.

Smith, S.D., 1980: Wind stress and heat flux over the ocean in gale force winds. *J Phys Oceanogr*, **10**, 709–726.

Spillane, M.C., Monahan, E.C., Bowyer, P.A., Doyle, D.M. and Stabeno, P.J., 1986: Whitecaps and global fluxes. *In* Monahan, E.C. and MacNiocaill, G. (eds), Oceanic whitecaps. Dordrecht, Reidel.
Stabeno, P.J. and Monahan, E.C., 1986: The influence of whitecaps on the albedo of the sea surface. *In* Monahan, E.C. and MacNiocaill, G. (eds), Oceanic whitecaps. Dordrecht, Reidel.
Wu, J., 1980: Wind-stress coefficients over the sea surface near neutral conditions — a revisit. *J Phys Oceanogr*, **10**, 727–740.

551.578.7:551.501.81:656.1(410.1)

Three motorway traffic accidents in hail showers on 29 March 1986: A radar study

W.S. Pike
19 Inholmes Common, Woodlands St Mary, Newbury, Berkshire RG16 7SX,

Summary

Heavy hail showers caused three major traffic accidents on English motorways when Easter saturday coincided with the last weekend in March 1986. The showers were sometimes accompanied by thunder and often moved quite rapidly at 30–40 m.p.h. The UK weather radar network was able to provide 15 minutes warning of the heaviest showers, and closer liaison with motorway police might eventually result in timely temporary use of speed-limit advisory signs along motorways in future similar situations.

1. Introduction

Holiday road traffic is often particularly dense on motorways, and Easter Saturday, 29 March 1986, was a typical example as drivers were encouraged to venture out in sunny weather during the morning over many central and eastern areas of the United Kingdom.

Three separate major traffic accidents, each involving carriageway-blocking 'pile-ups' of vehicles, occurred as dense and often fast-moving traffic ran into sudden heavy hail showers. These accidents are briefly analysed here together with the UK weather radar network 5 km data (at 15-minute intervals) to see what conclusions may be reached.

2. The synoptic situation

On 29 March 1986 the United Kingdom was affected by a fresh, unstable, westerly polar maritime airstream, in which showery troughs (see Figs 1(a) and 1(b)) were affecting western districts from mid-morning onwards, with clear skies and a deceptively sunny start in most other areas.

Towards midday a pool of very cold air with snow showers even at low levels was making rapid progress over Ireland, associated with a marked upper trough and a north-westerly 'jet streak' in the south. Over the United Kingdom showery surface troughs were generated both ahead of, and in association with, this cold air aloft. The visible image AVHRR satellite picture for 1328 UTC (not shown) gave a good indication of this troughing process which 'banked-up' successive bands of convective cloud over the United Kingdom ahead of more-open 'speckled' cells in the coldest air further west.

Ahead of the first trough the airflow backed west-south-westerly over much of England and the temperatures had risen rapidly to 11 °C at the surface in the south-eastern counties by late morning. Strong convective heating resulted in a scattering of relatively small but heavy showers, often falling as soft hail and occasionally accompanied by thunder, affecting all southern counties by 1145 UTC (see Fig. 2).

3. Radar interpretation

Five-kilometre squares might be considered as really too coarse a grid for accurate interpretation of shower intensities, which are sometimes known to give heavier falls than one is led to believe, in smaller areas. However, the 2 km radar has a lower extreme range (some 77 km) as opposed to the 210 km or so for the 5 km radar and, with quite deep convection involved, the latter network is preferred here.

Fig. 2 gives the radar precipitation rates, as averaged by computer, over 5 km squares at 1145 UTC on 29 March 1986. *Observer's Handbook* definitions of shower intensities do not completely agree with the intensity ranges indicated by the 5 km radar '10-level display scheme'. Therefore, the 'dot screens' used in Figs 3–5 have been interpreted as shown in Fig. 3.

Heavy intensities continued to be analysed throughout the afternoon and evening by the UK weather radar network before dying out later. Particularly violent showers and storms, with precipitation rates in excess of 64 mm h^{-1}, occurred near Evesham (Hereford and Worcester) and just south-west of Faversham (Kent) at

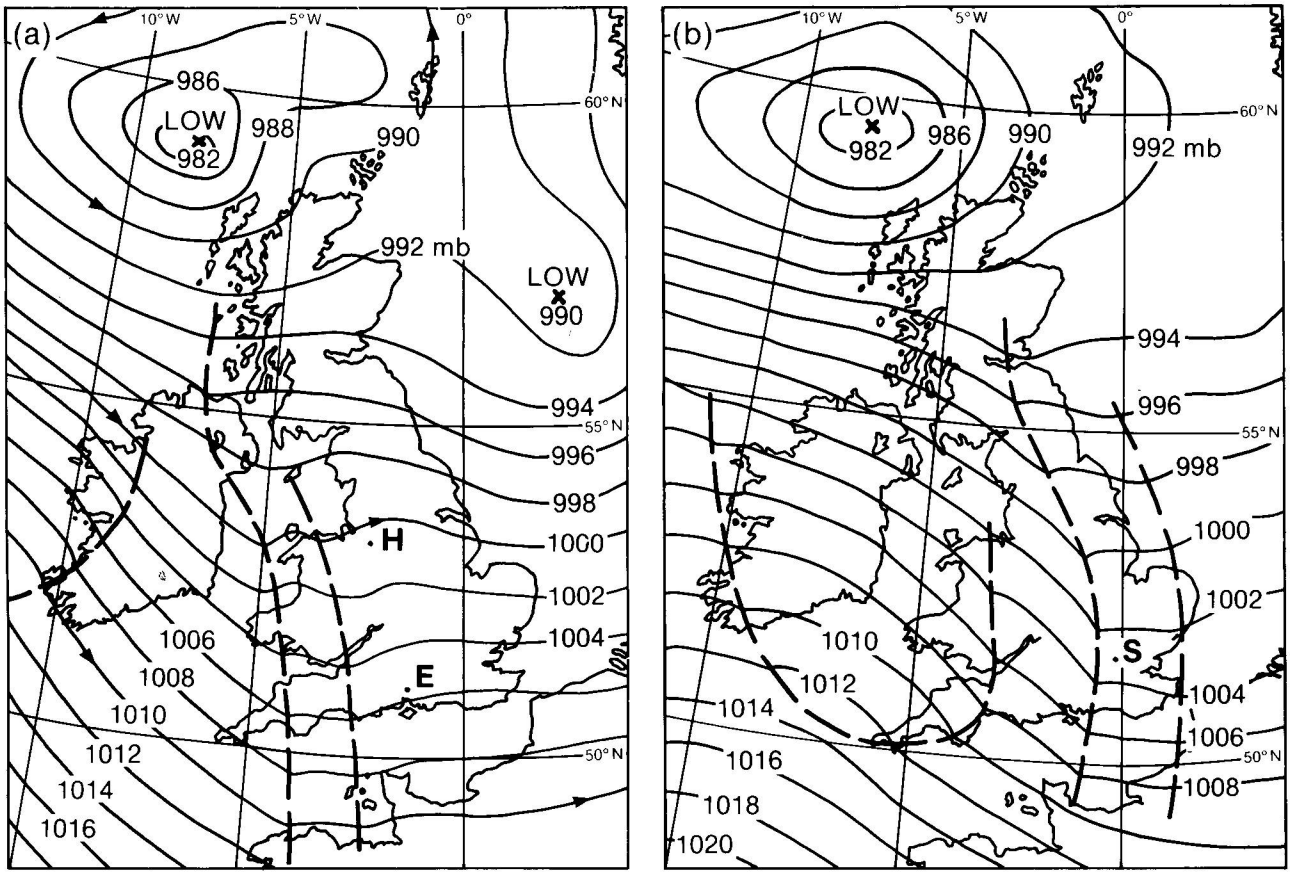

Figure 1. Surface synoptic charts for (a) 1200 UTC and (b) 1800 UTC on 29 March 1986. E, H and S show the locations of Eastleigh, Hassall and Scratchwood, respectively.

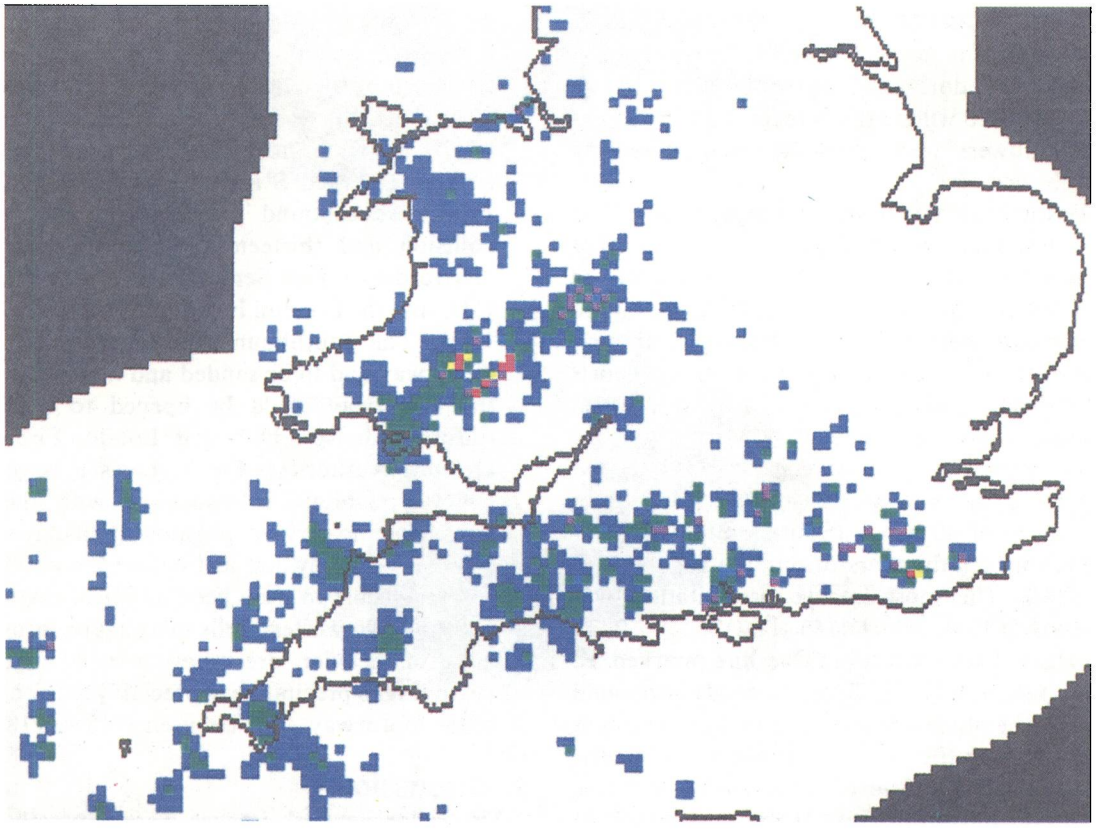

Figure 2. Rainfall distribution from the UK weather radar network at 1145 UTC on 29 March 1986. Rainfall intensities (mm h^{-1}) shown are: dark blue < 1, green 1–4, purple 4–8, light blue 8–16, pink 16–32 and yellow > 32.

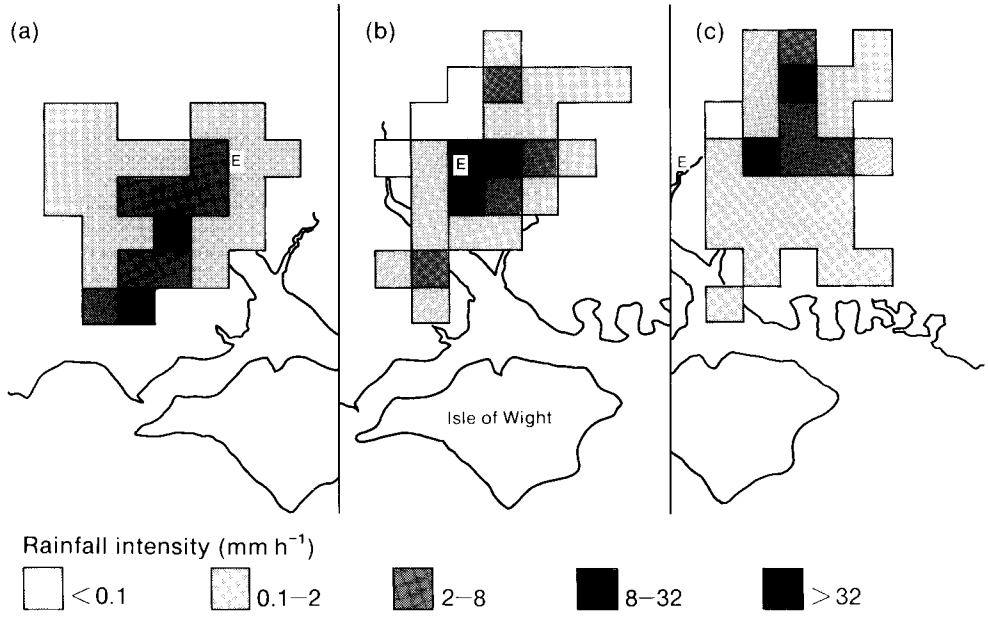

Figure 3. Data from the UK weather radar network at 5 km intervals around Eastleigh (marked E) at (a) 1130, (b) 1145 and (c) 1200 UTC on 29 March 1986. The location of Eastleigh is also shown in Fig. 1(a).

1400 UTC. Further violent storms were indicated near Cheshunt (Hertfordshire) and at Newmarket (Suffolk) by 1545 UTC. The latter East Anglian storms moved north-eastwards to affect the Ely and Thetford areas before decreasing in intensity after 1630 UTC, when approaching Norwich.

4. The traffic accidents

There were three major traffic accidents reported on English motorways during the course of the day, and all apparently occurred when drivers reacted differently as heavy hail showers were suddenly encountered by speeding vehicles:

(a) at Eastleigh, Hampshire (E on Figs 1(a) and 3) at approximately 12 noon near junction 5 of the M27 motorway. It resulted in temporary closure of the entire road. At first six westbound vehicles were involved but, immediately afterwards, four eastbound vehicles collided while attempting to avoid debris from the first accident which had crossed the central reservation. Apart from shock there were no serious injuries sustained. Fig. 3 shows this storm had moved rapidly from the west-south-west at an effective ground speed of 40 m.p.h. (Southampton Weather Centre reported a thunderstorm in the past hour at 1200 UTC). The most intense precipitation was indicated over Eastleigh at 1145 UTC).

(b) At Hassall near Alsager in Cheshire (marked 'H' in Figs 1(a) and 4) at 1237 UTC involving 34 northbound vehicles on the M6 motorway. There was no accident to southbound traffic which continued to flow freely. Fourteen people were injured (12 seriously) and were taken to North Staffordshire Hospital in a fleet of six ambulances. The northbound M6 was closed for nearly 3 hours after the accident. A spokesman from the Operational Support Division of the Cheshire Constabulary said 'The majority of drivers reduced speed in response to the weather conditions, the minority did not slow sufficiently and prosecutions took place for careless driving' (B. Ingham, Cheshire Constabulary, personal communication). Fig. 4 shows a relatively small but intense shower falling just west of Hassall at 1215 UTC, which then proceeded steadily in a north-easterly direction to pass just to the north of the village (and over the motorway) at 1230 UTC.

(c) At Edgware, north London, near Scratchwood Services (marked 'S' in Figs 1(b) and 5) at 1820 UTC. Fifteen southbound vehicles were involved in a collision and thirteen people were injured. The Hertfordshire Fire Service was summoned at 1824 UTC and the London Fire Brigade called out at 1827 UTC. The southbound carriageways of the M1 motorway had to be sanded and hosed down before the motorway could be opened to traffic again (information from D. Norris, London Fire and Civil Defence Authority). Fig. 5 shows a large area of heavy precipitation (associated with the second advancing showery trough) moving quickly eastwards towards Scratchwood just before the accident. The storm appears to have been a typical multicell type with the two western cells merging to form a larger area of heavier precipitation and another cell beginning to precipitate appreciably to the north-east of the motorway — all between 1745 and 1800 UTC.

5. Discussion

The radar network images were generally able to identify heavy precipitation occurring (albeit at this stage mostly in the cloud) from at least 15 minutes

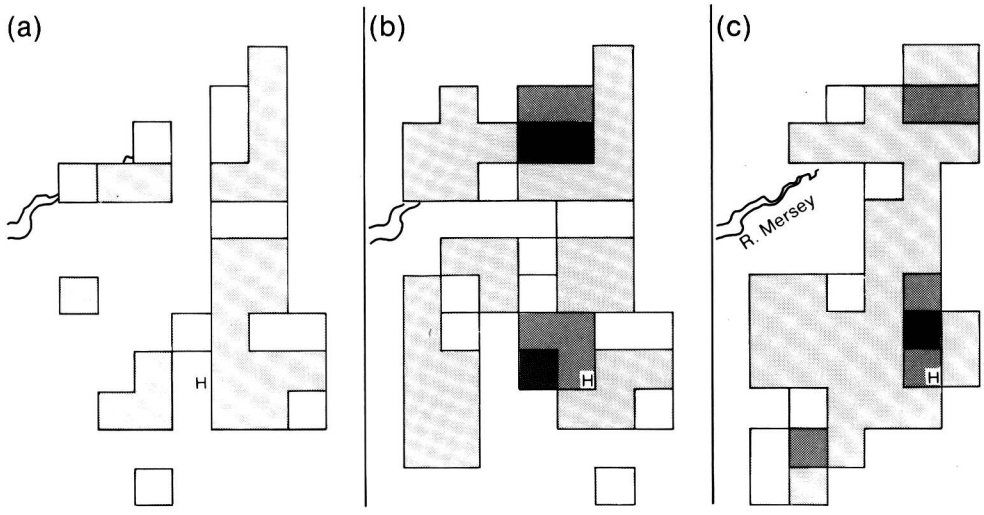

Figure 4. Data from the UK weather radar network at 5 km intervals around Hassall, Cheshire (marked H) at (a) 1200, (b) 1215 and (c) 1230 UTC on 29 March 1986. For intensities see Fig. 3. The location of Hassall is also shown in Fig. 1(a).

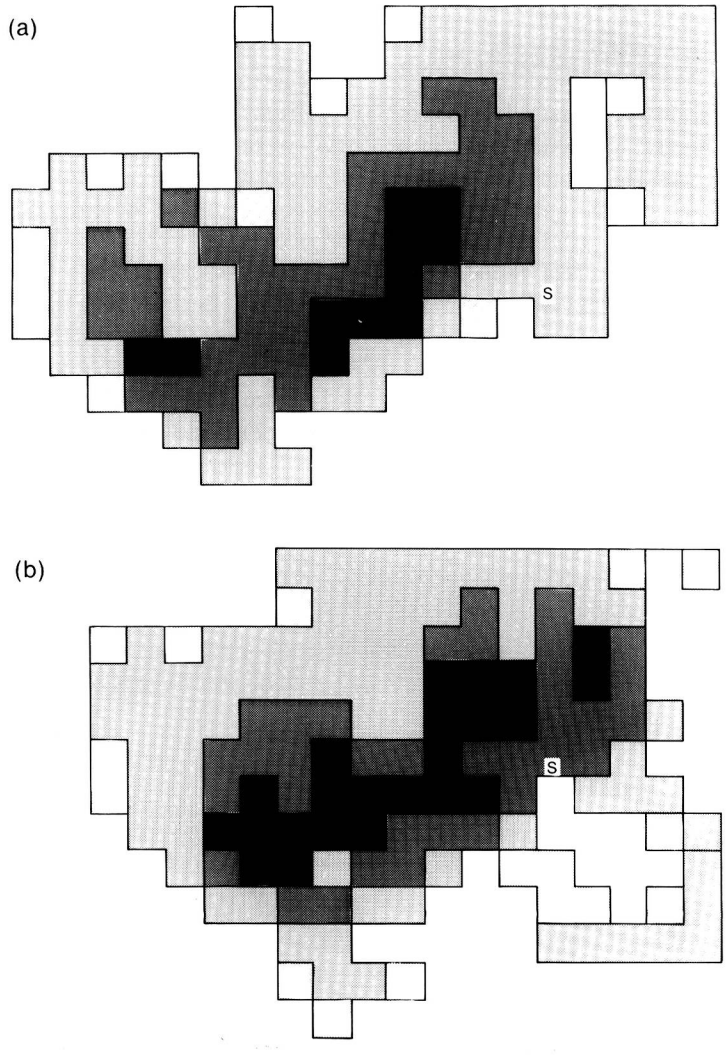

Figure 5. Data from the UK weather radar network at 5 km intervals around Scratchwood (marked S) at (a) 1745 and (b) 1800 UTC on 29 March 1986. For intensities see Fig. 3. The location of Scratchwood is also shown in Fig. 1(b).

before traffic accidents occurred, and such a period of notice could give motorway police and other emergency services a correspondingly useful period of warning as to where the heaviest precipitation is imminent. Speed restriction signs might be switched on temporarily.

At present the advice given by the Department of Transport (DTp) is for drivers to 'use common sense' in adverse weather conditions. However, 'common sense' varies considerably from driver to driver! As occurred in Cheshire, police prosecutions for careless driving may well result from collision with the vehicle in front if speed is not consciously and consistently reduced by each driver. However, the trauma of sudden noise and lack of visibility as one's vehicle runs into a heavy, squally hail shower, perhaps with a clap of thunder, all with a closing (i.e. combined) speed of sometimes in excess of 100 m.p.h., has been observed to result in the exact opposite reaction from some motorists who accelerate in a futile attempt to run through the trouble more rapidly and, hopefully, to come out into the sunshine once again!

It was established (R. Yarwood of the Road Safety Division of the DTp, personal communication) that a reduction of visibility to less than 100 m is officially recognized by the DTp and legal profession generally as being 'poor'.

When driving in poor visibility it is first advisable to check your vehicle's speedometer, as sudden entry into these conditions leads to a special danger of 'spatial disorientation' which can lead to people driving faster than they realize because of the lack of external visual references, which can disastrously affect the driver's judgement of speed and distance. The effect is more usually associated with sudden entry into a fog patch when drivers, similar to airline pilots flying into cloud, must suddenly rely on their instruments.

When encountering a heavy shower, especially of hail, which can instantly reduce visibility to that described as 'poor' above, another important question arises for the vehicle driver as to whether or not it is safer for them to stop for a time on the hard shoulder of the motorway, however briefly, to wait until the shower abates, or else to carry on driving at a much reduced speed and risk being struck from behind!

Because it is illegal (under Motorway Traffic Regulations 1982) to allow one's vehicle to rest on the hard shoulder of a motorway 'except in an emergency', on the basis that it is dangerous to stop near to the free-flowing traffic passing just a few feet away, it is again only officially recommended that drivers 'use common sense within the prevailing conditions'. However, it was conceded that when hail, road spray and greasy windscreens conspire to reduce visibility below 100 m 'it may be prudent for the driver to stop on the hard shoulder' (R. Yarwood, personal communication).

6. Conclusions

The UK weather radar network is usually capable of giving at least a few minutes notice of very heavy showers. Closer liaison with motorway police could lead to timely, temporary use of the recommended speed-limit warning signs, if these were spaced at intervals of 1 mile along carriageways (as emergency telephones are at present). This would help eliminate the 'commonsense' variable which drivers are currently urged to follow in adverse or 'poor' conditions, i.e. below 100 m. If conditions become particularly hazardous it may be prudent to stop on the hard shoulder until conditions improve because violent hail does constitute 'an emergency' due to the reduction in visibility.

Acknowledgements

Thanks to the following information sources: National Meteorological Library and Archives, Bracknell; British Newspaper Library, Colindale; Chief Superintendent B. Ingham, Cheshire Constabulary; Fireman D. Norris, London Fire and Civil Defence Authority; R. Yarwood, Road Safety Division, DTp, and G.A. Monk of the Meteorological Office for supplying the radar imagery.

Books received

The listing of books under this heading does not preclude a review in the Meteorological Magazine at a later date.

The engineering statistician's guide to continuous bivariate distributions, by T.P. Hutchinson and C.D. Lai (Adelaide, Rumsby Scientific Publishing, 1991. $A 44.00, $US 32.00) discusses the subject in various applications, including water in different situations. The ways in which the view of bivariate distributions has changed over recent years are explained. ISBN 0 646 024132.

Air pollution modeling and its application VIII, edited by H. van Dop and D.G. Steyn (New York, London, Plenum Press, 1991. $ 198.00) contains over one hundred papers given at the eighteenth International Technical Meeting 13–17 May 1990 in Vancouver. The authors were drawn from the worldwide scientific community. ISBN 0 306 43828 3.

GUIDE TO AUTHORS

Content

Articles on all aspects of meteorology are welcomed, particularly those which describe results of research in applied meteorology or the development of practical forecasting techniques.

Preparation and submission of articles

Articles, which must be in English, should be typed, double-spaced with wide margins, on one side only of A4-size paper. Tables, references and figure captions should be typed separately. Spelling should conform to the preferred spelling in the *Concise Oxford Dictionary* (latest edition). Articles prepared on floppy disk (IBM-compatible) can be labour-saving, but only a print-out should be submitted in the first instance.

References should be made using the Harvard system (author/date) and full details should be given at the end of the text. If a document is unpublished, details must be given of the library where it may be seen. Documents which are not available to enquirers must not be referred to, except by 'personal communication'.

Tables should be numbered consecutively using roman numerals and provided with headings.

Mathematical notation should be written with extreme care. Particular care should be taken to differentiate between Greek letters and Roman letters for which they could be mistaken. Double subscripts and superscripts should be avoided, as they are difficult to typeset and read. Notation should be kept as simple as possible. Guidance is given in BS 1991: Part 1: 1976, and *Quantities, Units and Symbols* published by the Royal Society. SI units, or units approved by the World Meteorological Organization, should be used.

Articles for publication and all other communications for the Editor should be addressed to: The Chief Executive, Meteorological Office, London Road, Bracknell, Berkshire RG12 2SZ and marked 'For Meteorological Magazine'.

Illustrations

Diagrams must be drawn clearly, preferably in ink, and should not contain any unnecessary or irrelevant details. Explanatory text should not appear on the diagram itself but in the caption. Captions should be typed on a separate sheet of paper and should, as far as possible, explain the meanings of the diagrams without the reader having to refer to the text. The sequential numbering should correspond with the sequential referrals in the text.

Sharp monochrome photographs on glossy paper are preferred; colour prints are acceptable but the use of colour is at the Editor's discretion.

Copyright

Authors should identify the holder of the copyright for their work when they first submit contributions.

Free copies

Three free copies of the magazine (one for a book review) are provided for authors of articles published in it. Separate offprints for each article are not provided.

Contributions: It is requested that all communications to the Editor and books for review be addressed to the Chief Executive, Meteorological Office, London Road, Bracknell, Berkshire RG12 2SZ, and marked 'For *Meteorological Magazine*'. Contributors are asked to comply with the guidelines given in the *Guide to authors* (above). The responsibility for facts and opinions expressed in the signed articles and letters published in *Meteorological Magazine* rests with their respective authors.

Subscriptions: Annual subscription £36.00 including postage; individual copies £3.25 including postage. Applications for postal subscriptions should be made to HMSO, PO Box 276, London SW8 5DT; subscription enquiries 071–873 8499.

Back numbers: Full-size reprints of Vols 1–75 (1866–1940) are available from Johnson Reprint Co. Ltd, 24–28 Oval Road, London NW1 7DX. Complete volumes of *Meteorological Magazine* commencing with volume 54 are available on microfilm from University Microfilms International, 18 Bedford Row, London WC1R 4EJ. Information on microfiche issues is available from Kraus Microfiche, Rte 100, Milwood, NY 10546, USA.

March 1992

Edited by R.M. Blackall
Editorial Board: R.J. Allam, R. Kershaw, W.H. Moores, P.R.S. Salter

Vol. 121
No. 1436

Contents

Page

Appointment of Chief Executive of the Meteorological Office. 57

Ocean Forecasting. Nina Morgan 58

An assessment of the surface fluxes from the Meteorological Office numerical weather prediction models. Part II. Heat and fresh water. J.O.S. Alves 59

Three motorway traffic accidents in hail showers on 29 March 1986: A radar study W.S. Pike 84

Books received 88

ISSN 0026–1149

ISBN 0-11-728981-7

9 780117 289819

Printed in the United Kingdom for HMSO
Dd291241 3/92 C13 503 12521